Brain-wide connectivity patterns of feedforward and feedback cortico-cortical neurons in the mouse secondary visual cortex

Richard G. Dickson[1], Matthew W. Jacobs[1], Alec L.R. Soronow[1], Faye An[1], Walid A. Yuqob[1], Euiseok J. Kim[1,2,3]*

[1]Department of Molecular, Cell, and Developmental Biology, University of California, Santa Cruz, CA 95064, USA

[2]Institute for the Biology of Stem Cells, University of California, Santa Cruz, CA 95064, USA

[3]Lead Contact

Running title: Brain-wide circuits for FF/FB neurons

*Corresponding Author: Euiseok J. Kim

Department of Molecular, Cell, and Developmental Biology, University of California, Santa Cruz, 1156 High Street, Santa Cruz, CA 95064, USA

Phone: 831-502-7233

Fax: 831-459-3139

ekim62@ucsc.edu

ACKNOWLEDGEMENTS

We thank Bin Chen, Bradley Colquitt, and David Feldheim for reading the manuscript and Efrain Hernandez Alvarez for mouse husbandry and histology. We thank undergraduate volunteers Eugene Kim, Jordan Chong, Hannah Tao, Lily Taylor-Hunt, Paul Pham, and Julian Swartz for tissue processing and histology. We acknowledge technical support from Benjamin Abrams, UCSC Life Sciences Microscopy Center, RRID: SCR_021135. Purchase of the Zeiss 880 confocal microscope used in this research was made possible through the National Institutes of Health s10 Grant 1S10OD23528-01. We acknowledge support from the UCSC start-up fund, the Whitehall Foundation, the Hellman Fellows Program, the E. Matilda Ziegler Foundation for the Blind, BRAIN Initiative at the National Institutes of Health RF1MH132591 and the National Institute of Neurological Disorders and Stroke at the National Institutes of Health, R01NS128771 (E.J.K.), the Koret scholar program (A.L.R.S.), and a National Institutes of Health IRACDA Postdoctoral Training Grant, K12GM139185 (R.G.D.).

ABSTRACT

Feedforward and feedback cortico-cortical neurons are distinct yet spatially intermingled subtypes distributed across cortical layers, playing specialized roles in sensory and cognitive processing. However, whether their presynaptic inputs differ to support these functions remains unknown. Using projection- and layer-specific monosynaptic rabies tracing, we mapped brain-wide long-distance inputs to multiple feedforward and feedback neuron types in VISl (also known as LM), the mouse secondary visual cortex. Overall, long-distance input patterns for these feedforward and feedback neurons were largely similar, as all received the majority of their inputs from VISp, the primary visual cortex, along with substantial inputs from various other cortical and visual thalamic regions. Despite their similarities, these feedforward and feedback types differed in the proportion of long-distance cortical inputs originating from specific visual, retrosplenial, and auditory cortices. These findings reveal the input connectivity patterns of cortico-cortical neurons based on feedforward and feedback projections, providing an anatomical framework for future studies on their functions and circuit integration.

KEYWORDS

cortical hierarchy, cortico-cortical neurons, feedforward and feedback neurons, mouse visual cortex, rabies tracing

KEY POINTS

1) Feedforward and feedback cortico-cortical projection neurons in VISl form largely distinct populations that are distributed across multiple cortical layers.

2) Four different feedforward and feedback cortico-cortical projection neuron types receive broadly similar patterns of long-distance input across the brain.

3) Despite overall similarities, feedforward and feedback neurons differ in the relative proportions of inputs from specific areas, including visual, retrosplenial, and auditory cortices.

INTRODUCTION

The mammalian cortex is responsible for high-level perception and cognition and is composed of numerous interconnected cortical areas (Felleman and Van Essen, 1991; Oh et al., 2014; Gămănuţ et al., 2018). These areas communicate through long-distance inter-areal connections mediated by excitatory cortico-cortical projection neurons (CCPNs). Two key organizational features of the mammalian cortex are its six-layered laminar structure and its hierarchical organization (Felleman and Van Essen, 1991; Cajal, 1995). Each cortical layer is considered as a different information-processing unit (Harris and Shepherd, 2015). CCPNs in a specific layer of each cortical area can be further divided into feedforward projection neurons, which send axons to higher-order cortical areas, and feedback projection neurons, which project to lower-order cortical areas. These two neuronal types are thought to process distinct types of information, feedforward neurons primarily transmitting sensory input from the external world and feedback neurons modulating contextual factors such as attention, brain states, and background information (Hupé et al., 1998; Nassi et al., 2013; Keller et al., 2020; Debes and Dragoi, 2023). Despite their distinct roles, these feedforward and feedback neurons are spatially intermingled within cortical layers (Berezovskii et al., 2011). Recent advances have elucidated their functional roles (Keller et al., 2020; Fişek et al., 2023), however, it remains unclear whether feedforward and feedback projection neurons within a specific layer of a given cortical area receive distinct or similar brain-wide presynaptic inputs. Uncovering this would provide insight into their proposed functional differences.

The mouse visual cortex serves as an ideal model for investigating the brain-wide connectivity of layer- and projection-specific cell types at a cellular level. This is due to the availability of viral genetic tools that enable precise labeling of neurons based on their axonal projections (e.g.,

retrograde tracer such as AAVretro) and laminar identity (e.g., layer-specific Cre-expressing transgenic mouse lines) (Gerfen et al., 2013; Tervo et al., 2016; Chatterjee et al., 2018; Matho et al., 2021). Additionally, the hierarchical organization of mouse visual cortical areas has been well characterized both anatomically and functionally (Harris et al., 2019; Siegle et al., 2021; D'Souza et al., 2022). The mouse visual cortex comprises the primary visual cortex (VISp) and at least ten different higher visual areas (HVAs), including the lateromedial (VISl) and posteromedial (VISpm) visual cortices (Wang and Burkhalter, 2007). In the cortical hierarchy, VISp represents the lowest level, VISl occupies an intermediate position, and VISpm is at a higher level (Harris et al., 2019; D'Souza et al., 2022). Within this framework, CCPNs in VISl that project to VISpm are defined as feedforward neurons, whereas those projecting to VISp are defined as feedback neurons (D'Souza et al., 2022). This makes VISl particularly suitable for studying spatially intermingled feedforward and feedback CCPNs.

Previous studies have mapped the monosynaptic inputs of layer-specific excitatory neuronal types (Vélez-Fort et al., 2014; DeNardo et al., 2015; Kim et al., 2015, 2020; Yao et al., 2023a). These studies suggest that long-distance input connectivity to specific layer-defined neuronal classes can be either distinct or largely comparable and that local connectivity varies (DeNardo et al., 2015; Yao et al., 2023a). However, it remains unclear whether feedforward and feedback CCPNs within the same cortical layer receive distinct brain-wide monosynaptic inputs, highlighting a critical gap in our understanding of cortical circuit organization.

To investigate the brain-wide monosynaptic input connectivity of layer-specific feedforward and feedback CCPNs in the mouse visual cortex, we employed the intersectional G-deleted rabies tracing method - cTRIO (cell-type specific inputs and outputs relationship) (Schwarz et al., 2015). Using an intersectional approach that combined layer-specific Cre recombinase with

111 projection-specific tTA trans-activator expression, we defined distinct subtypes of feedforward
112 and feedback CCPNs in layer 2/3 (L2/3) and 5 (L5) of VISl. We then mapped their long-distance
113 monosynaptic inputs using rabies tracing, leveraging two avian receptors, TVA and TVA^{66T}, for
114 avian sarcoma leukosis virus glycoprotein EnvA (Wickersham et al., 2007; Miyamichi et al.,
115 2013). Thus we are able to trace the monosynaptic inputs to neuronal subtypes which were
116 previously inaccessible to brainwide mapping efforts. Our findings reveal that while the overall
117 input patterns to L2/3 and L5 feedforward and feedback CCPNs in VISl are largely comparable,
118 there are notable differences in the proportions of long-distance inputs from the visual, auditory,
119 and retrosplenial cortices. The experimental design presented here provides a framework for
120 investigating hierarchical brain-wide networks across different species and brain structures
121 beyond the mouse visual cortex. This study also provides a comprehensive presynaptic input
122 connectivity map that will serve as a foundation for future experimental and theoretical
123 investigations into cortico-cortical neuronal functions.
124

125 **MATERIALS AND METHODS**

126 **Resource and materials availability**

127 Further information and requests for resources and materials should be directed to and will be
128 fulfilled by the lead contact, Euiseok J. Kim (ekim62@ucsc.edu). Microscopy and any additional
129 data reported in this paper will be shared by the lead contact upon reasonable request.
130

131 **Experimental animals**

132 GENSAT BAC transgenic *SepW1-Cre* NP39 and *Tlx3-Cre* PL56 mouse lines have been
133 previously described (Gerfen et al., 2013). The transgenic mice were maintained on C57BL/6J

134 backgrounds. C57BL/6J mice were used as wild-type. Both male and female mice were used. All
135 mice were housed with a 12-hour light and 12-hour dark cycle and *ad libitum* access to food and
136 water. All animal procedures were performed in accordance with the University of California,
137 Santa Cruz animal care and use committee (IACUC)'s regulations.
138
139 **Virus preparation**
140 All adeno-associated viruses (AAVs) and SAD B19 EnvA-pseudotyped glycoprotein (G)-deleted
141 rabies virus (EnvA+RVdG) were produced by the Salk Viral Core GT3: scAAVretro-hSyn-BFP
142 ($1.26X10^{12}$ GC/ml), scAAVretro-hSyn-H2B-eGFP ($1.16X10^{13}$ GC/ml), scAAVretro-hSyn-H2B-
143 mCherry ($1.21X10^{13}$ GC/ml), AAVretro-nEF-lox66/71-tTA ($4.8X10^{13}$ GC/ml), AAV8-TRE-
144 DIO-oG ($5.92X10^{12}$ GC/ml), AAV8-TRE-DIO-eGFP-T2A-TVA ($7.00X10^{13}$ GC/ml), AAV8-
145 TRE-DIO-TVA^{66T}eGFP-P2A-oG ($7.40X10^{13}$ GC/ml), and EnvA+RVdG-mCherry ($7.71X10^{8}$-
146 $1.43X10^{10}$) Infectious Unit (IU)/ml).
147
148 **Animal surgery for virus injection**
149 For all surgeries anesthesia induction was with 100 mg/kg of ketamine and 10 mg/kg of xylazine
150 cocktail via intraperitoneal injections, and anesthesia was maintained as needed with ~1%
151 isoflurane. Mice were mounted in a stereotax (RWD instruments) for surgery and stereotaxic
152 injections. For rabies tracing experiments, *SepW1-Cre* NP39 or *Tlx3-Cre* PL56 mice received
153 AAV helper injections at postnatal day (P)63-P125. 50-200 nl of AAVretro-nEF-lox66/71-tTA
154 was injected into the center of the medial secondary visual cortex (VISpm), primary visual
155 cortex (VISp), or anterior cingulate area (ACA) using the following coordinates: 1.6 mm rostral,
156 1.5 mm lateral relative to lambda and 0.4-0.6 mm ventral from the pia for VISpm or 1.1 mm

157 rostral, 2.6 mm lateral to lambda and 0.45-0.67 mm ventral from the pia for VISp, 0.4 mm
158 rostral, 0.4 mm lateral to bregma and 0.7-0.8 mm ventral from the pia for ACA. A 50 nl mixture
159 of 9:1 AAV8-TRE-DIO-oG and AAV8-TRE-DIO-eGFP-T2A-TVA, a 50 nl mixture of 2:7:1
160 AAV8-TRE-DIO-oG, 1x PBS and AAV8-TRE-DIO-eGFP-T2A-TVA, or 50 nl of AAV8-TRE-
161 DIO-TVA^{66T}eGFP-P2A-oG was injected into the center of the lateral secondary visual cortex
162 (VISl), using the following coordinates: 0.7 mm rostral, 3.65 mm lateral relative to lambda and
163 0.4-0.6 mm ventral from the pia. We injected AAVs using air pressure using a 1 ml syringe with
164 18G tubing adaptor and tubing. To prevent virus backflow, the pipette was left in the brain for 5-
165 10 minutes after the completion of the injection. After recovery, mice were given water with
166 ibuprofen (30 mg/kg) and subcutaneous carprofen (5 mg/kg). Two weeks after AAV helper
167 injection, 100 nl of EnvA+RVdG-mCherry was injected into the same site in VISl using a 1 ml
168 syringe-mediated air pressure. After recovery, mice were again given water with ibuprofen (30
169 mg/kg) and subcutaneous carprofen (5 mg/kg) and housed for seven days to allow for trans-
170 synaptic rabies spread and fluorescent protein expression.

171 For retrograde colocalization studies, mice were prepared and head-fixed as previously with the
172 same coordinates for VISpm, VISp, and ACA as above. For triple AAV colocalization
173 experiments, combination of 50-100 nl of scAAVretro-hSyn-BFP, scAAVretro-hSyn-H2B-
174 mCherry, scAAVretro-hSyn-H2B-eGFP were injected into one of VISp, VISpm, and ACA.
175 AAV was left to express for 18-21 days before the tissue harvest and histology. For VISpm/VISp
176 colocalization experiments, 50-100 nl of cholera toxin subunit B conjugated to Alexa fluor 647
177 (CTB-647, 1 mg/ml, Invitrogen C34778), Alexa fluor 555 (CTB-555, 1 mg/ml, Invitrogen
178 C22843) and/or Alexa fluor 488 (CTB-488, 1 mg/ml, Invitrogen C34775) was injected into

179 VISpm, VISp, and/or ACA, respectively. Three or four days later, the tissue was harvested for
180 histology. Detailed information of injections on individual mice can be found in Table 1.
181
182 **Histology and image analysis**

183 Brains were harvested after trans-cardiac perfusion using phosphate-buffered saline (PBS)
184 followed by 4% paraformaldehyde (PFA). Brains were dissected out from skulls and post-fixed
185 with 2% PFA and 15% sucrose in PBS at 4°C overnight and then immersed in 30% sucrose in
186 PBS at 4°C before sectioning. Using a freezing microtome, 50-100 µm coronal brain sections
187 were cut and stored in cryogen (30% ethylene glycol, 30% glycerol, 30% ddH_20, 10% 10x PBS)
188 at 4°C, every other section was stained and mounted for data analysis and quantification. Before
189 staining, sections were washed 3x 10 minutes in PBS and permeabilized and blocked in PBS/5%
190 normal donkey serum (Millipore S30-100ML)/1% Triton-X 100 (Sigma-Aldrich X100-100ML)
191 for two hours at room temperature. To enhance eGFP and mCherry signals, free-floating sections
192 were incubated at 4°C overnight with goat anti-GFP (1:1000; Rockland 600-101-215,
193 RRID:AB_218182) and rabbit anti-dsRed (1:500; Clontech 632496, RRID:AB_10013483)
194 primary antibodies in PBS/0.5% normal donkey serum/0.1% Triton-X 100, followed by 3x 10
195 minutes in PBS wash and incubation with the appropriate secondary antibodies conjugated with
196 Alexa 488 or 568 (1:500; Invitrogen A-11055 (RRID:AB_2534102) or A-10042
197 (RRID:AB_2534017), respectively). Sections were counterstained with 10 µM DAPI (4',6-
198 diamidino-2-phenylindole) in PBS for 30 minutes to visualize cell nuclei, followed by 3x 10
199 minutes in PBS wash. Immunostained tissue sections were mounted on slides with a polyvinyl
200 alcohol mounting medium containing DABCO (PVA-DABCO) and allowed to air-dry overnight.

201 All sections were scanned with a 10x/0.45 NA (wd-2.0 mm) objective on a Zeiss AxioImager Z2
202 Widefield Microscope using tile scan and Z-stack (every 6-8 µm). Representative images were
203 taken with the Zeiss 880 Confocal Microscope with 10x/0.45 NA (wd-2.0 mm) or 40x/ 0.95 NA
204 corr (wd-0.25 mm) objectives. Scanned images were first processed in Zeiss ZEN 3.11 with
205 DAPI images for alignment and fluorescent images for eGFP+ or mCherry+ cell detections
206 exported for processing. Subsequent image files were processed and analyzed using Bell Jar for
207 long-distance input mapping (Soronow et al., 2025). For alignment, the center Z-stack DAPI
208 images were used to predict the section's xy coordinates and cut angle for alignment to the Allen
209 Brain Common Coordinate Framework reference atlas (Wang et al., 2020). Alignments were
210 then fine-tuned in Bell Jar to ensure fit and minimize counting rabies-labeled cells resulting from
211 minor TVA expression leakage in non-Cre-expressing neurons (Wall et al., 2010). Layers for
212 VISpm and VISp were also manually fine-tuned to ensure accuracy. The exported Zeiss ZEN
213 files with mCherry+ signals were used for automated cell counting. Using Bell Jar, max
214 projection images were produced from the Z-stacks, and these max projections were then
215 sharpened in the program before detection. Detection thresholds were kept stable unless manual
216 counting validation showed less than 90% accuracy of cell labeling, in which case the confidence
217 interval was adjusted (three out of 15 brains) to ensure accurate counting. Cell detection and
218 brain alignment were then integrated, and the long-distance ipsi-hemispheric cortical input
219 fractions were calculated and graphed using GraphPad Prism 10.1.1. For thalamic input
220 proportions, areas and cells were drawn and counted manually on Zeiss ZEN 3.11 using the
221 Allen Brain Common Coordinate Framework reference atlas (Wang et al., 2020).
222
223 **Quantification and Statistical analysis**

224 The values of n and what n represents are reported in results and figure legends. For statistical
225 significance, two-way ANOVA with Tukey's multiple comparisons test was performed with
226 GraphPad Prism 10.1.1. A one-way ANOVA with the Fisher's Least Significant Difference
227 (LSD) post hoc for multiple comparisons test was performed using IBM SPSS 30. Unless
228 otherwise noted, statistical significance is indicated as follows: *$p < 0.05$; **$p < 0.01$; ***$p <$
229 0.001; ****$p < 0.0001$. In Fig. 4C, significance is denoted differently: *(black) $p < 0.05$ and
230 *(magenta) $p < 0.01$.
231

232 **RESULTS**

233 **Feedforward and feedback cortico-cortical projection neurons of VISl are largely non-**
234 **overlapping and distributed across layers**

235 We first investigated the long-distance projection targets of CCPNs in VISl using published data
236 from the Allen Mouse Brain Connectivity Atlas (Harris et al., 2019). This dataset provides high-
237 resolution maps of eGFP+ axonal projections in adult mouse brains, generated by injecting
238 AAV1-CAG-FLEx-eGFP into Cre-expressing transgenic mice to label specific neuronal
239 populations in different brain regions. To examine CCPNs in VISl, we analyzed data from *Cux2-*
240 *IRES-Cre* and *Tlx3-Cre* mice, which label layers 2-4 (L2-4) and L5 CCPNs, respectively. Whole-
241 brain projection maps revealed that both L2-4 and L5 CCPNs extend axons to more than 13
242 cortical areas, including visual areas as VISp, VISpm, and VISpor and non-visual areas such as
243 the temporal association cortex (TEa) and the anterior cingulate area, dorsal part (ACAd) (Fig.
244 1A-B). Quantitative analysis of the axonal projection volumes across these regions showed that
245 L2-4 and L5 CCPNs exhibit similar projection patterns, with the highest projection volume in
246 VISp (39.43 ± 3.20% in *Cux2-IRES-Cre* and 29.75 ± 3.80% in *Tlx3-Cre*, mean ± SEM),

247 followed by VISpm, VISpor, VISli, and VISrl (Fig. 1B). Notably, L2-4 CCPNs exhibit sparse
248 axonal projections to ACAs (1.10 ± 0.28%), whereas 3.55 ± 0.95% of the total axonal
249 projections from L5 CCPNs target ACAd (Fig. 1B).

250 Next, we investigated whether CCPNs in VISl that project to three major cortical target areas
251 (VISp, ACA/MOs (secondary motor cortex), and VISpm) represent distinct or overlapping cell
252 types at the single-cell level. To retrogradely label these projection neurons with three different
253 fluorescent markers, we stereotaxically injected AAVretro-hSyn-H2B-mCherry into VISp,
254 AAVretro-hSyn-BFP into ACA/MOs, and AAVretro-hSyn-H2B-eGFP into VISpm in wild-type
255 adult C57BL/6J mice (Fig. 1C). Thus, VISl neurons projecting to VISpm, VISp, and
256 ACA/MOs—designated as VISl→VISpm, VISl→VISp, and VISl→ACA, respectively. In VISl
257 of these mice, labeled CCPNs were distributed across layers 2-6. The majority of neurons were
258 labeled by a single fluorescent protein (VISl→VISpm 90.97 ± 2.08%, VISl→VISp 92.25 ±
259 5.04%, VISl→ACA 87.94 ± 4.60%, n = 2 mice) with relatively few exhibiting double or triple
260 labeling (Fig. 1C). These findings indicate that CCPNs projecting to VISpm or ACA/MOs
261 (feedforward, FF) and VISp (feedback, FB) do not extensively share axonal collaterals consistent
262 with a previous study (Berezovskii et al., 2011). Therefore, VISl→VISpm, VISl→VISp, and
263 VISl→ACA CCPNs are largely distinct neuronal subpopulations.
264

265 **Brain-wide monosynaptic input mapping of feedforward and feedback CCPNs in VISl**

266 We examined whether long-distance inputs to feedforward and feedback neurons align with one
267 of three possible organizational models (Fig. 2A). In Model 1, these neurons receive inputs from
268 the same areas they project to, establishing a reciprocal connectivity pattern that facilitates
269 looped computations. In Model 2, feedforward and feedback neurons differ in the type of

information they relay; feedforward neurons preferentially receive inputs from lower sensory areas such as VISp and the dorsal lateral geniculate nucleus of the thalamus (LGd), while feedback neurons receive inputs from higher cortical areas that convey contextual information such as higher cortical areas and the lateral posterior thalamic nucleus (LP). In Model 3, both feedforward and feedback neurons receive inputs from the same brain regions, making them anatomically indistinguishable. In this scenario, despite similar long-distance anatomical inputs, feedforward and feedback neurons may exhibit distinct functional roles due to differences in local circuit computations. Alternatively, the long-distance inputs themselves may differ functionally, even if their anatomical connectivity proportion from each brain region appears similar.

To differentiate between these three models, we mapped and characterized the brain-wide long-distance inputs to distinct feedforward and feedback CCPNs in VISl. We implemented an intersectional rabies tracing strategy called cTRIO to map monosynaptic inputs in a projection- and layer-specific manner. We first injected a helper virus mixture of AAV8-TRE-DIO-oG (rabies glycoprotein) (Kim et al., 2016) and AAV8-TRE-DIO-eGFP-T2A-TVA into VISl, along with AAVretro-nEF-lox66/71-tTA (hereafter AAVretro-tTA) into projection targets, including VISpm, VISp, and ACA, in L2/3-specific *SepW1-Cre* or L5 CCPN-specific *Tlx3-Cre* transgenic mice (Gerfen et al., 2013). This ensured Cre- and tTA-dependent expression of the avian TVA receptor and rabies glycoprotein (oG). This approach enabled selective labeling of feedforward and feedback neurons in L2/3 or L5 (Fig. 2D). 14 days later, EnvA-pseudotyped glycoprotein (G)-deleted rabies virus (EnvA+RVdG)-mCherry was injected into the same VISl location to enable monosynaptic input tracing from the starter neurons. After seven days, brains were harvested, sectioned, immunostained with goat anti-eGFP (Rockland 600-101-215,

293 RRID:AB_218182) and rabbit anti-dsRed (Clontech 632496, RRID:AB_10013483) antibodies,
294 and imaged to quantify brain-wide long-distance inputs.
295
296 **Control experiments to optimize layer- and projection-specific monosynaptic rabies tracing**

297 We conducted a series of experiments to optimize our monosynaptic rabies tracing approach.
298 Our goal was to minimize false-positive long-distance labeling and prevent contamination of the
299 starter neuron population. Such issues could arise from 'leaky' expression of transgenes such as
300 TVA and oG independent of Cre and tTA activity (Wall et al., 2010; Lavin et al., 2020), as well
301 as from unintended damage to long-distance axonal tracts in the white matter (Watakabe and
302 Hirokawa, 2018) (Fig. 3).

303 To examine the absence of false-positive long-distance rabies labeling, we first injected AAV8-
304 TRE-DIO-eGFP-T2A-TVA (without oG) into VISl and AAVretro-tTA into VISp of *Tlx3-Cre*
305 mice (Fig. 3A). 14 days later, we administered EnvA+RVdG-mCherry into VISl and harvested
306 the brains seven days post-injection (Fig. 3A). As expected, in the absence of oG, no mCherry+
307 rabies-labeled neurons were detected outside of the injection site (VISl) (Fig. 3B-B').

308 In additional controls, we injected either a mixture of AAV8-TRE-DIO-eGFP-T2A-TVA and
309 AAV8-TRE-DIO-oG (Fig. 3C), or AAV8-TRE-DIO-TVA^{66T}eGFP-P2A-oG alone (Fig. 3E) into
310 VISl or VISp, but without AAVretro-tTA injections. In both cases, following EnvA+RVdG-
311 mCherry and a seven-day incubation period, no mCherry+ rabies-labeled neurons outside of the
312 injection site (Fig. 3C-D', E-F')

313 Next, to assess the purity of starter neurons and verify whether L2/3 or L5 VISl→VISp CCPNs
314 contained only VISl→VISp neurons, we injected AAV8-TRE-DIO-TVA^{66T}eGFP-P2A-oG into

315 VISl and a mixture of AAVretro-tTA and Alexa Fluor 647-conjugated cholera toxin subunit B
316 (CTB) into VISp of *Tlx3-Cre* mice (Fig. 3G-H), and collected brains three weeks later. Confocal
317 imaging showed that TVA^{66T}eGFP-P2A-oG labeled L5 neurons in VISl were also labeled with
318 CTB, showing that they were VISl→VISp neurons (Fig. 3H).

319 To determine whether VISl→VISpm neurons were included in the L2/3 VISl→VISp starter
320 population due to passing axons in the grey matter of lower cortical layers (Watakabe and
321 Hirokawa, 2018), we injected AAV8-TRE-DIO-TVA^{66T}eGFP-P2A-oG into VISl, AAVretro-tTA
322 into VISp, and CTB into VISpm of *SepW1-Cre* mice (Fig. 3I-J). Confocal images of brain
323 sections harvested three weeks later showed that TVA^{66T}eGFP-P2A-oG expressing neurons were
324 not labeled with CTB, indicating that virus-labeled starter neurons did not include VISl→VISpm
325 neurons (Fig. 3J). These experiments validate our approach, ensuring specificity in identifying
326 monosynaptic inputs while preventing false positives and potential starter population
327 contamination.

328 **Long-distance cortical inputs onto four different CCPN types in VISl**

329 We examined whether the four types of feedforward and feedback CCPNs (L2/3 VISl→VISpm,
330 L2/3 VISl→VISp, L5 VISl→VISpm, L5 VISl→VISp) in VISl receive similar or distinct
331 monosynaptic inputs from other cortical areas within the ipsilateral hemisphere (Fig. 4 and Table
332 2). Rabies-labeled long-distance input neurons to those four types of CCPNs were distributed
333 throughout both visual and non-visual cortical areas (Fig. 4A), with the highest proportion
334 originating from VISp (L2/3 VISl→VISpm 0.409 ± 0.046, L2/3 VISl→VISp 0.380 ± 0.030, L5
335 L5 VISl→VISpm 0.492 ± 0.016, L5 VISl→VISp 0.582 ± 0.023, Fig. 4B). We quantified and
336 ranked the top 20 cortical regions contributing inputs along the cortical hierarchy (Harris et al.,

337 2019). While overall input patterns among the four CCPN types were largely similar, we
338 identified key differences. L5 VISl→VISp feedback neurons received a greater proportion of
339 long-distance inputs from VISp compared to L5 VISl→VISpm feedforward neurons (Fig. 4B).
340 Similarly, L2/3 VISl→VISpm feedforward neurons received a significantly greater proportion of
341 their inputs from VISpm than L2/3 VISl→VISp feedback neurons (Fig. 4C).

342 Further statistical analysis using one-way ANOVA revealed that at least one of the four CCPN
343 types exhibited a significantly different proportional input than other CCPNs in eight out of the
344 20 cortical areas analyzed (Fig. 4C): VISpm, VISpl, AUDd, AUDp, RSPv, RSPagl, RSPd, and
345 MOs. Overall, these findings suggest that while the four CCPN types receive broadly
346 comparable long-distance cortical inputs, they exhibit distinct preferences for specific cortical
347 regions, reflecting their functional roles in cortical processing. Notably, L5 VISl→VISpm
348 CCPNs receive proportionally more retrosplenial cortex input, suggesting a greater role in visuo-
349 spatial memory, and L2/3 CCPNs regardless of projection receive proportionally more auditory
350 cortex input suggesting a greater role for L2/3 CCPNs in audio-visual integration (Fig. 4B-C).

351 We next investigated the laminar distribution of long-distance presynaptic inputs from VISp and
352 VISpm to four distinct types of feedforward and feedback CCPNs in VISl. Although prior
353 studies have reported preferential long-distance connectivity between superficial layers and
354 between deep layers (DeNardo et al., 2015; Kim et al., 2015), it remains unclear whether CCPNs
355 in specific layers of a given cortical area receive layer-specific long-distance inputs, depending
356 on their feedforward or feedback projections. To address this, we quantified the proportion of
357 input neurons across each layer of VISp and VISpm (Fig. 5A-B) for four distinct CCPN types in
358 VISl: L2/3 VISl→VISpm, L2/3 VISl→VISp, L5 VISl→VISpm, and L5 VISl→VISp. With a

359 few exceptions, the laminar distribution of input neurons in VISp and VISpm did not reveal
360 statistically significant differences across these neuronal groups (Fig. 5A-B).

361 We investigated whether feedforward neurons in VISl that project to cortical areas with higher
362 hierarchy scores than VISpm exhibit more distinct input connectivity patterns from those of
363 VISl→VISp compared to VISl→VISpm neurons. Previous studies have shown that the cortical
364 hierarchy in rodents is relatively shallow compared to that of primates (Harris et al., 2019;
365 D'Souza et al., 2022). The hierarchy scores based on layer-termination patterns of cortico-
366 cortical connection (Harris et al., 2019) for select cortical areas are as follows: VISp: -0.239,
367 VISl: -0.148, VISpm: 0.074, ACAd: -0.060, ACAv: 0.404, and MO: 0.282., To determine if the
368 shallow hierarchy in the mouse visual cortex was masking hierarchy dependent input differences,
369 we injected AAVretro-tTA into ACA/MOs and a mixture of AAV8-TRE-DIO-oG and AAV8-
370 TRE-DIO-eGFP-T2A-TVA into VISl of *Tlx3-Cre* mice to label VISl→ACA/MOs (hereafter,
371 VISl→ACA) neurons and traced their monosynaptic inputs across the cortex. We then compared
372 these results with monosynaptic input tracing of L5 VISl→VISpm feedforward neurons and L5
373 VISl→VISp feedback neurons (Fig. 5C). We found broadly similar input connectivity profiles
374 across these three L5 CCPN subtypes. Thus, the input connectivity of L5 VISl→ACA CCPNs is
375 comparable to that of VISl→VISpm CCPNs and does not exhibit greater differences from
376 VISl→VISp CCPNs than from VISl→VISpm CCPNs. Notably, the proportion of inputs from
377 VISp to VISl→VISp neurons was higher than that to VISl→VISpm and VISl→ACA neurons
378 (Fig. 5C).

379 **Long-distance thalamic input neuron profiles onto four different CCPN types in VISl**

380 Next, we examined whether the four types of feedforward and feedback CCPNs in VISl receive
381 distinct presynaptic inputs from visual thalamic regions. In the mouse visual system, LGd

382 projects to VISl and other higher visual cortical areas in addition to VISp, while LP and the
383 laterodorsal nucleus of the thalamus (LD) also provide input to VISl and other visual cortical
384 regions (Bienkowski et al., 2019).

385 In rabies-traced brain sections, we identified three thalamic nuclei, LGd, LD, and LP, and
386 quantified the proportion of rabies-labeled neurons among all these input areas (Fig. 6A). Across
387 all four CCPN types, LP provided the majority of thalamic inputs, followed by LGd and LD,
388 consistent with a previous study (Yao et al., 2023a) (Fig. 6B). While the overall proportions of
389 thalamic inputs were similar, we observed that L2/3 VISl→VISpm neurons received a lower
390 proportion of inputs from LGd compared to L5 VISl→VISpm neurons (L2/3 VISl→VISpm:
391 0.102 ± 0.008 and L5 VISl→VISpm 0.323 ± 0.027, p=0.0030, two-way ANOVA with Tukey's
392 multiple comparisons test) (Fig. 6B). Conversely, L2/3 VISl→VISpm neurons received a higher
393 proportion of inputs from LP than L5 VISl→VISpm neurons (L2/3 VISl→VISpm 0.887 ± 0.004,
394 L5 VISl→VISpm 0.657 ± 0.024, p=0.0021, two-way ANOVA with Tukey's multiple
395 comparisons test) (Fig. 6B).

396

397 **DISCUSSION**

398 Using a layer- and projection-specific monosynaptic rabies tracing approach, we mapped brain-
399 wide inputs to five distinct types of feedforward and feedback CCPNs in VISl. This study
400 provides the first comprehensive connectivity maps to investigate the organizational principles
401 governing feedforward and feedback neurons in relation to their laminar positions and the
402 hierarchical positions of their target areas. Our findings indicate that long distance input
403 connectivity patterns are largely comparable across CCPN subtypes, supporting Model 3 (Fig.

404 2A), but notable differences emerge based on their laminar and projection identities. First, L2/3
405 VISl→VISpm CCPNs received a higher proportion of inputs from their own projection target,
406 VISpm, compared to L2/3 VISl→VISp and other L5 CCPNs. Similarly, L5 VISl→VISp CCPNs
407 received a higher proportion of inputs from VISp, their projection target, compared to L5
408 VISl→VISpm or VISl→ACA CCPNs. These results are in accordance with Model 1 (Fig. 2A),
409 in which monosynaptic inputs preferentially originate from the neurons' axonal targets (Kim et
410 al., 2020; Siu et al., 2021). These insights provide a foundation for future functional and
411 theoretical studies aimed at understanding brain-wide cortical computations at the cellular level.

412 The input-output organization of neural networks provides crucial insights into the information
413 they receive and the signals they transmit for functional processing. Therefore, understanding
414 neuronal connectivity patterns is essential for a comprehensive understanding of neural circuit
415 function and computation (Zeng and Sanes, 2017). Previous studies have demonstrated that
416 distinct neuronal cell types in the mammalian brain exhibit characteristic input connectivity
417 patterns. Even within broader neuronal classes, spatially intermingled subtypes display subtype-
418 specific input connectivity (e.g., dopaminergic D1 receptor versus D2 receptor expressing spiny
419 projection neurons in the striatum or serotonergic neuron subtypes in the dorsal raphe; see also
420 whole-brain rabies tracing data) (Wall et al., 2016; Ren et al., 2018). A recent study found that
421 functionally distinct neuronal types in layer 2/3 of the mouse somatosensory cortex exhibit
422 distinct brain-wide input connectivity patterns (Inácio et al., 2025). For cortico-cortical
423 connectivity in the visual cortices, a previous study found that VISp CCPNs projecting to VISpm
424 or VISal received inputs from the same respective areas, suggesting a like-to-like connectivity
425 pattern (Kim et al., 2020). A previous study observed laminar differences in like-to-like
426 connectivity using Channelrhodopsin-2-assisted circuit mapping, where there is stronger like-to-

427 like connectivity in L5 compared to L2/3 neurons (Young et al., 2021). This observation of like-
428 to-like connectivity is further supported by a study in macaques, where V1 neurons projecting to
429 V2 receive monosynaptic feedback inputs from V2 but not from other V1-projecting areas (Siu
430 et al., 2021). In the mouse VISl, the secondary visual cortex, projection-specific input
431 connectivity is observed, though it appears less pronounced than in CCPNs of VISp, the primary
432 visual cortex. One possible explanation is that VISl→VISpm and VISl→VISp neurons share
433 similar medial axonal projection trajectories, whereas VISp→VISpm and VISp→VISal (VISp
434 CCPNs projecting to anterolateral, AL, visual cortex) neurons exhibit medial versus lateral
435 projection patterns. Another, not mutually exclusive, possibility is that the cortical hierarchy in
436 the mouse visual system is relatively shallow, making it more challenging to detect strong
437 hierarchical connectivity features.

438 To validate the projection identities of our starter neurons, we used CTB injections into both
439 target and non-target projection areas (Fig. 3G-J). However, given the collateralization properties
440 of some CCPNs (Han et al., 2018; Peng et al., 2021), it remains possible that certain starter
441 neurons project to additional areas beyond our intended target regions, including both VISpm
442 and VISp. This could introduce variability in rabies tracing results and complicate efforts to
443 restrict analyses to exclusive starter populations.

444 Monosynaptic rabies tracing is a powerful approach for mapping anatomical connections across
445 the brain; however, this method does not provide information about synaptic strength or other
446 functional properties of these connections (Callaway and Luo, 2015). For example, although
447 feedforward and feedback CCPNs may receive similar proportions of inputs from a given area, it
448 remains unclear whether these input neurons are functionally distinct—for example, whether
449 they exhibit different receptive field properties or belong to different functional subtypes. To

450 gain additional insight into the functional differences and similarities between feedforward and
451 feedback CCPNs, future studies could complement rabies tracing with electrophysiological or
452 imaging approaches. Additionally, advances in high-throughput molecular profiling, including
453 single-cell RNA sequencing, have revealed that cortical neurons within a single layer can be
454 further classified into distinct subtypes based on unsupervised clustering (Tasic et al., 2018; Yao
455 et al., 2023b). Beyond their broad excitatory versus inhibitory or laminar identities, it would be
456 valuable to examine whether long-distance input neurons exhibit specific connectivity patterns
457 among these molecularly defined subtypes of CCPNs (Condylis et al., 2022).

458 It is also possible that, despite receiving similar long-distance inputs, feedforward and feedback
459 neurons differ in their local circuit architecture. To further test Model 3 (Fig. 2A) and uncover
460 additional anatomical distinctions, future studies using TVA^{66T}-dependent rabies tracing for local
461 inputs, combined with molecular characterization of input neurons and electrophysiological
462 profiling would be informative.

463 In this study, we used feedforward and feedback CCPNs in the VISl as a model to investigate
464 connectivity differences. A key question for future research is whether similar connectivity
465 profiles would be observed in other cortical regions, such as secondary somatosensory cortex
466 projecting to primary somatosensory cortex as feedback CCPNs and secondary somatosensory
467 cortex projecting to primary and secondary motor cortices as feedforward CCPNs (Yamashita et
468 al., 2018). Given that the cortical hierarchy in mice is relatively shallow compared to that of
469 higher mammals (Harris et al., 2019; D'Souza et al., 2022), it would also be interesting to
470 explore these questions in species with a more robust hierarchical organization, such as
471 marmosets or macaques.
472

Declaration of Interests

The authors declare no competing interests that could have influenced the contents of this publication.

FIGURE LEGENDS

Figure 1. Whole-brain distributions of axonal projections from VISl CCPNs. (A) Top-down views of whole-brain 3D reconstructions of axonal projections from VISl. (Top) L2-4 CCPNs in a *Cux2-IRES-Cre* brain (Experiment: 287495026). (Bottom) L5 CCPNs in a *Tlx3-Cre* brain (Experiment: 520750912). Data adapted from the Allen Brain Connectivity Atlas (https://connectivity.brain-map.org/projection). **(B)** Percentage of total axon projection volume across 13 cortical areas from L2-4 VISl CCPNs in *Cux2-IRES-Cre* (magenta, n = 2) and L5 VISl CCPNs in *Tlx3-Cre* (cyan, n = 3). **(C)** Confocal microscope images showing the injection sites of AAVretro-H2B-eGFP, AAVretro-H2B-mCherry, and AAVretro-BFP targeting ACAd/MO, VISp, and VISpm, respectively. Allen Reference Atlas (ARA) section numbers are in the top left corner. **(D)** Representative confocal microscope images showing VISl CCPNs retrogradely labeled based on their axonal projections to ACAd/MO, VISp, or VISpm. Arrows indicate neurons that project to more than one of these target areas. Data are represented as mean ± SEM.

Figure 2. Long-distance connectivity models and projection- and layer-specific rabies tracing strategy. (A) Three proposed models of long-distance monosynaptic input connectivity to feedforward (FF) and feedback (FB) neurons. **(B)** Schematic of the intersectional rabies tracing strategy for projection- and layer-specific long-distance input tracing to VISl neurons. **(C)** Representative scanning microscope images overlaid with the Allen Brain Common Coordinate Framework reference atlas (Wang et al., 2020), showing AAVretro-tTA targeting in three different areas: VISpm, VISp, and ACA. **(D)** Representative confocal microscope images showing eGFP+mCherry+ starter neurons (arrowheads) in VISl projecting to VISp, VISpm, and ACA in *SepW1-Cre* or *Tlx3-Cre* mice.

Figure 3. Control brains. (A) Schematic of the viral genetic tracing strategy for control injections without oG (rabies glycoprotein). **(B)** Fluorescence microscope images showing the absence of labeled cells outside the injection sites **(B')**. **(C,E)** Schematic of the viral genetic tracing strategy for control injections without tTA. **(D-D', F-F')** Fluorescence microscope images showing the absence of labeled cells outside the injection sites **(D', F')**. **(G, I)** Schematic of the viral genetic tracing strategy used to verify the axonal projection targets of labeled starter neurons (TVA^{66T}eGFP-P2A-oG+) by CTB injections into either the expected projection target, VISp **(G-H)**, or a non-target area, VISpm **(I-J)**. **(H)** Yellow arrowheads indicate starter neurons co-labeled with eGFP (cyan) and CTB (magenta), indicating their axonal projections to VISp.

Figure 4. Long-distance input mapping of layer- and projection-specific CCPNs in VISl. (A) Representative confocal images showing long-distance mCherry+ input neurons in LP, VISp, VISpm, and RSP for four distinct feedforward and feedback CCPN types in VISl of *SepW1-Cre* or *Tlx3-Cre* mice. **(B)** The ipsilateral cortical proportion of input neurons across 20 cortical areas, sorted by cortical hierarchy (Harris et al., 2019). The red arrowhead indicates the rank of VISl along the cortical hierarchy. n = 3 mice per each group. Two-way ANOVA with Tukey's multiple comparisons test, * $p<0.05$, ** $p<0.01$, *** $p<0.001$, **** $p<0.0001$. **(C)** Results of one-way ANOVA with Fisher's Least Significant Difference (LSD) post-hoc test for eight selected input regions. *(black) $p<0.05$, *(magenta) $p<0.01$. Data are represented as mean ± SEM.

Figure 5. Further analyses of long-distance input neurons to CCPNs in VISl. (A) The distributions of presynaptic input neurons across VISp layers to four distinct types of CCPNs in VISl. **(B)** The distribution of presynaptic input neurons across VISpm layers to four distinct types of CCPNs in VISl. **(C)** The proportion of long-distance input neurons located in each of the 20 cortical regions for the three L5 CCPN types in VISl. n = 3 mice per each group for each figure. Two-way ANOVA with Tukey's multiple comparisons test, * $p<0.05$, ** $p<0.01$, **** $p<0.0001$. Data are represented as mean ± SEM.

Figure 6. Long-distance thalamic input mapping of layer- and projection-specific CCPNs in VISl. (A) Representative confocal microscope images showing rabies-labeled mCherry+ input neurons in LGd

522 or LP. **(B)** Proportions of long-distance inputs from each visual thalamic region to four distinct types of
523 feedforward and feedback starter neurons in VISl. n = 3 mice per each group. Two-way ANOVA with
524 Tukey's multiple comparisons test, * $p<0.05$. Data are represented as mean ± SEM.

525 **Table 1. Animal and experimental condition summary**

526 **Table 2. Quantification of rabies tracing in individual mouse brains**

527 **Abbreviations**: AAV, Adeno associated virus; ACA, Anterior cingulate area; ACAd, Anterior cingulate
528 area dorsal; ACAv, Anterior cingulate area ventral; Alp, Agranular insular area, posterior part; AUDd,
529 Dorsal auditory area; AUDp, Primary auditory area; AUDpo, Posterior auditory area; AUDv, Ventral
530 auditory area; CCPN, Cortico-cortical projection neurons; CTB, Cholera toxin subunit B; cTRIO, Cell
531 specific tracing the relationship between input and output; ECT, Ectorhinal area; ENTl, Entorhinal area,
532 lateral part; ENTm, Entorhinal area, medial part, dorsal zone; EnvA, Envelope protein of avian leukosis
533 virus; FB, feedback neurons; FF, feedforward neurons; GU, Gustatory areas; HVA, Higher visual area;
534 LD, Lateral dorsal nucleus of thalamus; LGd, Lateral geniculate nucleus dorsal; LP, Lateral posterior
535 nucleus of the thalamus; Mop, Primary motor area; Mos, Secondary motor cortex; oG, optimized rabies
536 glycoprotein; ORBl, Orbital area, lateral part; PBS, Phosphate buffered saline; PERI, Perirhinal area;
537 PFA, paraformaldehyde; RSP, Retrosplenial cortex; RSPagl, Retrosplenial cortex agranular; RSPd,
538 Retrosplenial cortex dorsal; RSPv, Retrosplenial cortex ventral; SSp-bfd, Primary somatosensory area,
539 barrel field; SSp-ll, Primary somatosensory area, lower limb; SSp-m, Primary somatosensory area,
540 mouth; SSp-n, Primary somatosensory area, nose; SSp-ul, Primary somatosensory area, upper limb; SSp-
541 un, Primary somatosensory area, unassigned; SSp-tr, Primary somatosensory area, trunk; SSs,
542 Supplemental somatosensory area; TEa, Temporal association area; tTa, Tetracycline trans activator;
543 TVA, Receptor for avian leukosis virus; VISa, Anterior area secondary visual cortex; VISal,
544 Anterolateral secondary visual cortex; VISam, Anteromedial secondary visual cortex; VISC, Visceral
545 area; VISl (LM), Lateral secondary visual cortex; VISli, Latero intermediate secondary visual cortex;
546 VISp, Primary visual cortex; VISpl, Posterolateral secondary visual cortex; VISpm, Posteromedial
547 secondary visual cortex; VISpor, Postrhinal secondary visual cortex; VISrl, Rostrolateral secondary visual
548 cortex.

549

550 **REFERENCES**

551 Berezovskii VK, Nassi JJ, Born RT. 2011. Segregation of feedforward and feedback projections in mouse
552 visual cortex. J Comp Neurol 519:3672–3683.

553 Bienkowski MS, Benavidez NL, Wu K, Gou L, Becerra M, Dong H-W. 2019. Extrastriate connectivity of
554 the mouse dorsal lateral geniculate thalamic nucleus. J Comp Neurol 527:1419–1442.

555 Cajal SR y. 1995. Cajal's histology of the nervous system of man and vertebrates. New York, NY:
556 Oxford University Press.

557 Callaway EM, Luo L. 2015. Monosynaptic circuit tracing with glycoprotein-deleted rabies viruses. J
558 Neurosci 35:8979–8985.

559 Chatterjee S, Sullivan HA, MacLennan BJ, Xu R, Hou Y, Lavin TK, Lea NE, Michalski JE, Babcock KR,
560 Dietrich S, Matthews GA, Beyeler A, Calhoon GG, Glober G, Whitesell JD, Yao S, Cetin A, Harris
561 JA, Zeng H, Tye KM, Reid RC, Wickersham IR. 2018. Nontoxic, double-deletion-mutant rabies
562 viral vectors for retrograde targeting of projection neurons. Nat Neurosci 21:638–646.

563 Condylis C, Ghanbari A, Manjrekar N, Bistrong K, Yao S, Yao Z, Nguyen TN, Zeng H, Tasic B, Chen
564 JL. 2022. Dense functional and molecular readout of a circuit hub in sensory cortex. Science
565 375:eabl5981.

566 Debes SR, Dragoi V. 2023. Suppressing feedback signals to visual cortex abolishes attentional
567 modulation. Science 379:468–473.

568 DeNardo LA, Berns DS, DeLoach K, Luo L. 2015. Connectivity of mouse somatosensory and prefrontal
569 cortex examined with trans-synaptic tracing. Nat Neurosci 18:1687–1697.

570 D'Souza RD, Wang Q, Ji W, Meier AM, Kennedy H, Knoblauch K, Burkhalter A. 2022. Hierarchical and
571 nonhierarchical features of the mouse visual cortical network. Nat Commun 13:503.

572 Felleman DJ, Van Essen DC. 1991. Distributed hierarchical processing in the primate cerebral cortex.
573 Cereb Cortex 1:1–47.

574 Fişek M, Herrmann D, Egea-Weiss A, Cloves M, Bauer L, Lee T-Y, Russell LE, Häusser M. 2023.
575 Cortico-cortical feedback engages active dendrites in visual cortex. Nature 617:769–776.

576 Gămănuţ R, Kennedy H, Toroczkai Z, Ercsey-Ravasz M, Van Essen DC, Knoblauch K, Burkhalter A.
577 2018. The mouse cortical connectome, characterized by an ultra-dense cortical graph, maintains
578 specificity by distinct connectivity profiles. Neuron 97:698–715.e10.

579 Gerfen CR, Paletzki R, Heintz N. 2013. GENSAT BAC cre-recombinase driver lines to study the
580 functional organization of cerebral cortical and basal ganglia circuits. Neuron 80:1368–1383.

581 Han Y, Kebschull JM, Campbell RAA, Cowan D, Imhof F, Zador AM, Mrsic-Flogel TD. 2018. The logic
582 of single-cell projections from visual cortex. Nature 556:51–56.

583 Harris JA, Mihalas S, Hirokawa KE, Whitesell JD, Choi H, Bernard A, Bohn P, Caldejon S, Casal L, Cho
584 A, Feiner A, Feng D, Gaudreault N, Gerfen CR, Graddis N, Groblewski PA, Henry AM, Ho A,
585 Howard R, Knox JE, Kuan L, Kuang X, Lecoq J, Lesnar P, Li Y, Luviano J, McConoughey S,
586 Mortrud MT, Naeemi M, Ng L, Oh SW, Ouellette B, Shen E, Sorensen SA, Wakeman W, Wang Q,
587 Wang Y, Williford A, Phillips JW, Jones AR, Koch C, Zeng H. 2019. Hierarchical organization of

588 cortical and thalamic connectivity. Nature 575:195–202.

589 Harris KD, Shepherd GMG. 2015. The neocortical circuit: themes and variations. Nat Neurosci 18:170–
590 181.

591 Hupé JM, James AC, Payne BR, Lomber SG, Girard P, Bullier J. 1998. Cortical feedback improves
592 discrimination between figure and background by V1, V2 and V3 neurons. Nature 394:784–787.

593 Inácio AR, Lam KC, Zhao Y, Pereira F, Gerfen CR, Lee S. 2025. Brain-wide presynaptic networks of
594 functionally distinct cortical neurons. Nature:1–11.

595 Keller AJ, Roth MM, Scanziani M. 2020. Feedback generates a second receptive field in neurons of the
596 visual cortex. Nature 582:545–549.

597 Kim EJ, Jacobs MW, Ito-Cole T, Callaway EM. 2016. Improved monosynaptic neural circuit tracing
598 using engineered rabies virus glycoproteins. Cell Rep 15:692–699.

599 Kim EJ, Juavinett AL, Kyubwa EM, Jacobs MW, Callaway EM. 2015. Three types of cortical layer 5
600 neurons that differ in brain-wide connectivity and function. Neuron 88:1253–1267.

601 Kim EJ, Zhang Z, Huang L, Ito-Cole T, Jacobs MW, Juavinett AL, Senturk G, Hu M, Ku M, Ecker JR,
602 Callaway EM. 2020. Extraction of Distinct Neuronal Cell Types from within a Genetically
603 Continuous Population. Neuron 107:274–282.e6.

604 Lavin TK, Jin L, Lea NE, Wickersham IR. 2020. Monosynaptic tracing success depends critically on
605 helper virus concentrations. Front Synaptic Neurosci 12:6.

606 Matho KS, Huilgol D, Galbavy W, He M, Kim G, An X, Lu J, Wu P, Di Bella DJ, Shetty AS,
607 Palaniswamy R, Hatfield J, Raudales R, Narasimhan A, Gamache E, Levine JM, Tucciarone J,
608 Szelenyi E, Harris JA, Mitra PP, Osten P, Arlotta P, Huang ZJ. 2021. Genetic dissection of the
609 glutamatergic neuron system in cerebral cortex. Nature 598:182–187.

610 Miyamichi K, Shlomai-Fuchs Y, Shu M, Weissbourd BC, Luo L, Mizrahi A. 2013. Dissecting local
611 circuits: parvalbumin interneurons underlie broad feedback control of olfactory bulb output. Neuron
612 80:1232–1245.

613 Nassi JJ, Lomber SG, Born RT. 2013. Corticocortical feedback contributes to surround suppression in V1
614 of the alert primate. J Neurosci 33:8504–8517.

615 Oh SW, Harris JA, Ng L, Winslow B, Cain N, Mihalas S, Wang Q, Lau C, Kuan L, Henry AM, Mortrud
616 MT, Ouellette B, Nguyen TN, Sorensen SA, Slaughterbeck CR, Wakeman W, Li Y, Feng D, Ho A,
617 Nicholas E, Hirokawa KE, Bohn P, Joines KM, Peng H, Hawrylycz MJ, Phillips JW, Hohmann JG,
618 Wohnoutka P, Gerfen CR, Koch C, Bernard A, Dang C, Jones AR, Zeng H. 2014. A mesoscale
619 connectome of the mouse brain. Nature 508:207–214.

620 Peng H, Xie P, Liu L, Kuang X, Wang Y, Qu L, Gong H, Jiang S, Li A, Ruan Z, Ding L, Yao Z, Chen C,
621 Chen M, Daigle TL, Dalley R, Ding Z, Duan Y, Feiner A, He P, Hill C, Hirokawa KE, Hong G,
622 Huang L, Kebede S, Kuo H-C, Larsen R, Lesnar P, Li L, Li Q, Li X, Li Y, Li Y, Liu A, Lu D, Mok
623 S, Ng L, Nguyen TN, Ouyang Q, Pan J, Shen E, Song Y, Sunkin SM, Tasic B, Veldman MB,
624 Wakeman W, Wan W, Wang P, Wang Q, Wang T, Wang Y, Xiong F, Xiong W, Xu W, Ye M, Yin
625 L, Yu Y, Yuan J, Yuan J, Yun Z, Zeng S, Zhang S, Zhao S, Zhao Z, Zhou Z, Huang ZJ, Esposito L,
626 Hawrylycz MJ, Sorensen SA, Yang XW, Zheng Y, Gu Z, Xie W, Koch C, Luo Q, Harris JA, Wang

627 Y, Zeng H. 2021. Morphological diversity of single neurons in molecularly defined cell types.
628 Nature 598:174–181.

629 Ren J, Friedmann D, Xiong J, Liu CD, Ferguson BR, Weerakkody T, DeLoach KE, Ran C, Pun A, Sun
630 Y, Weissbourd B, Neve RL, Huguenard J, Horowitz MA, Luo L. 2018. Anatomically defined and
631 functionally distinct dorsal raphe serotonin sub-systems. Cell 175:472–487.e20.

632 Schwarz LA, Miyamichi K, Gao XJ, Beier KT, Weissbourd B, DeLoach KE, Ren J, Ibanes S, Malenka
633 RC, Kremer EJ, Luo L. 2015. Viral-genetic tracing of the input-output organization of a central
634 noradrenaline circuit. Nature 524:88–92.

635 Siegle JH, Jia X, Durand S, Gale S, Bennett C, Graddis N, Heller G, Ramirez TK, Choi H, Luviano JA,
636 Groblewski PA, Ahmed R, Arkhipov A, Bernard A, Billeh YN, Brown D, Buice MA, Cain N,
637 Caldejon S, Casal L, Cho A, Chvilicek M, Cox TC, Dai K, Denman DJ, de Vries SEJ, Dietzman R,
638 Esposito L, Farrell C, Feng D, Galbraith J, Garrett M, Gelfand EC, Hancock N, Harris JA, Howard
639 R, Hu B, Hytnen R, Iyer R, Jessett E, Johnson K, Kato I, Kiggins J, Lambert S, Lecoq J,
640 Ledochowitsch P, Lee JH, Leon A, Li Y, Liang E, Long F, Mace K, Melchior J, Millman D,
641 Mollenkopf T, Nayan C, Ng L, Ngo K, Nguyen T, Nicovich PR, North K, Ocker GK, Ollerenshaw
642 D, Oliver M, Pachitariu M, Perkins J, Reding M, Reid D, Robertson M, Ronellenfitch K, Seid S,
643 Slaughterbeck C, Stoecklin M, Sullivan D, Sutton B, Swapp J, Thompson C, Turner K, Wakeman
644 W, Whitesell JD, Williams D, Williford A, Young R, Zeng H, Naylor S, Phillips JW, Reid RC,
645 Mihalas S, Olsen SR, Koch C. 2021. Survey of spiking in the mouse visual system reveals functional
646 hierarchy. Nature 592:86–92.

647 Siu C, Balsor J, Merlin S, Federer F, Angelucci A. 2021. A direct interareal feedback-to-feedforward
648 circuit in primate visual cortex. Nat Commun 12:4911.

649 Soronow ALR, Jacobs MW, Dickson RG, Kim EJ. 2025. Bell Jar: A semiautomated registration and cell
650 counting tool for mouse neurohistology analysis. eNeuro [Internet] 12. Available from:
651 http://dx.doi.org/10.1523/ENEURO.0036-23.2025

652 Tasic B, Yao Z, Graybuck LT, Smith KA, Nguyen TN, Bertagnolli D, Goldy J, Garren E, Economo MN,
653 Viswanathan S, Penn O, Bakken T, Menon V, Miller J, Fong O, Hirokawa KE, Lathia K, Rimorin C,
654 Tieu M, Larsen R, Casper T, Barkan E, Kroll M, Parry S, Shapovalova NV, Hirschstein D,
655 Pendergraft J, Sullivan HA, Kim TK, Szafer A, Dee N, Groblewski P, Wickersham I, Cetin A,
656 Harris JA, Levi BP, Sunkin SM, Madisen L, Daigle TL, Looger L, Bernard A, Phillips J, Lein E,
657 Hawrylycz M, Svoboda K, Jones AR, Koch C, Zeng H. 2018. Shared and distinct transcriptomic cell
658 types across neocortical areas. Nature 563:72–78.

659 Tervo DGR, Hwang B-Y, Viswanathan S, Gaj T, Lavzin M, Ritola KD, Lindo S, Michael S, Kuleshova
660 E, Ojala D, Huang C-C, Gerfen CR, Schiller J, Dudman JT, Hantman AW, Looger LL, Schaffer DV,
661 Karpova AY. 2016. A designer AAV variant permits efficient retrograde access to projection
662 neurons. Neuron 92:372–382.

663 Vélez-Fort M, Rousseau CV, Niedworok CJ, Wickersham IR, Rancz EA, Brown APY, Strom M, Margrie
664 TW. 2014. The stimulus selectivity and connectivity of layer six principal cells reveals cortical
665 microcircuits underlying visual processing. Neuron 83:1431–1443.

666 Wall NR, De La Parra M, Sorokin JM, Taniguchi H, Huang ZJ, Callaway EM. 2016. Brain-wide maps of
667 synaptic input to cortical interneurons. J Neurosci 36:4000–4009.

668 Wall NR, Wickersham IR, Cetin A, De La Parra M, Callaway EM. 2010. Monosynaptic circuit tracing in

669 vivo through Cre-dependent targeting and complementation of modified rabies virus. Proc Natl Acad
670 Sci U S A 107:21848–21853.

671 Wang Q, Burkhalter A. 2007. Area map of mouse visual cortex. J Comp Neurol 502:339–357.

672 Wang Q, Ding S-L, Li Y, Royall J, Feng D, Lesnar P, Graddis N, Naeemi M, Facer B, Ho A, Dolbeare T,
673 Blanchard B, Dee N, Wakeman W, Hirokawa KE, Szafer A, Sunkin SM, Oh SW, Bernard A,
674 Phillips JW, Hawrylycz M, Koch C, Zeng H, Harris JA, Ng L. 2020. The Allen Mouse Brain
675 Common Coordinate Framework: A 3D reference atlas. Cell 181:936–953.e20.

676 Watakabe A, Hirokawa J. 2018. Cortical networks of the mouse brain elaborate within the gray matter.
677 Brain Struct Funct 223:3633–3652.

678 Wickersham IR, Lyon DC, Barnard RJO, Mori T, Finke S, Conzelmann K-K, Young JAT, Callaway EM.
679 2007. Monosynaptic restriction of transsynaptic tracing from single, genetically targeted neurons.
680 Neuron 53:639–647.

681 Yamashita T, Vavladeli A, Pala A, Galan K, Crochet S, Petersen SSA, Petersen CCH. 2018. Diverse
682 long-range axonal projections of excitatory layer 2/3 neurons in mouse barrel cortex. Front
683 Neuroanat 12:33.

684 Yao S, Wang Q, Hirokawa KE, Ouellette B, Ahmed R, Bomben J, Brouner K, Casal L, Caldejon S, Cho
685 A, Dotson NI, Daigle TL, Egdorf T, Enstrom R, Gary A, Gelfand E, Gorham M, Griffin F, Gu H,
686 Hancock N, Howard R, Kuan L, Lambert S, Lee EK, Luviano J, Mace K, Maxwell M, Mortrud MT,
687 Naeemi M, Nayan C, Ngo N-K, Nguyen T, North K, Ransford S, Ruiz A, Seid S, Swapp J, Taormina
688 MJ, Wakeman W, Zhou T, Nicovich PR, Williford A, Potekhina L, McGraw M, Ng L, Groblewski
689 PA, Tasic B, Mihalas S, Harris JA, Cetin A, Zeng H. 2023a. A whole-brain monosynaptic input
690 connectome to neuron classes in mouse visual cortex. Nat Neurosci 26:350–364.

691 Yao Z, van Velthoven CTJ, Kunst M, Zhang M, McMillen D, Lee C, Jung W, Goldy J, Abdelhak A,
692 Aitken M, Baker K, Baker P, Barkan E, Bertagnolli D, Bhandiwad A, Bielstein C, Bishwakarma P,
693 Campos J, Carey D, Casper T, Chakka AB, Chakrabarty R, Chavan S, Chen M, Clark M, Close J,
694 Crichton K, Daniel S, DiValentin P, Dolbeare T, Ellingwood L, Fiabane E, Fliss T, Gee J,
695 Gerstenberger J, Glandon A, Gloe J, Gould J, Gray J, Guilford N, Guzman J, Hirschstein D, Ho W,
696 Hooper M, Huang M, Hupp M, Jin K, Kroll M, Lathia K, Leon A, Li S, Long B, Madigan Z, Malloy
697 J, Malone J, Maltzer Z, Martin N, McCue R, McGinty R, Mei N, Melchor J, Meyerdierks E,
698 Mollenkopf T, Moonsman S, Nguyen TN, Otto S, Pham T, Rimorin C, Ruiz A, Sanchez R, Sawyer
699 L, Shapovalova N, Shepard N, Slaughterbeck C, Sulc J, Tieu M, Torkelson A, Tung H, Valera
700 Cuevas N, Vance S, Wadhwani K, Ward K, Levi B, Farrell C, Young R, Staats B, Wang M-QM,
701 Thompson CL, Mufti S, Pagan CM, Kruse L, Dee N, Sunkin SM, Esposito L, Hawrylycz MJ,
702 Waters J, Ng L, Smith K, et al. 2023b. A high-resolution transcriptomic and spatial atlas of cell types
703 in the whole mouse brain. Nature 624:317–332.

704 Young H, Belbut B, Baeta M, Petreanu L. 2021. Laminar-specific cortico-cortical loops in mouse visual
705 cortex. Elife [Internet] 10. Available from: http://dx.doi.org/10.7554/eLife.59551

706 Zeng H, Sanes JR. 2017. Neuronal cell-type classification: challenges, opportunities and the path forward.
707 Nat Rev Neurosci 18:530–546.

708

Figure 1

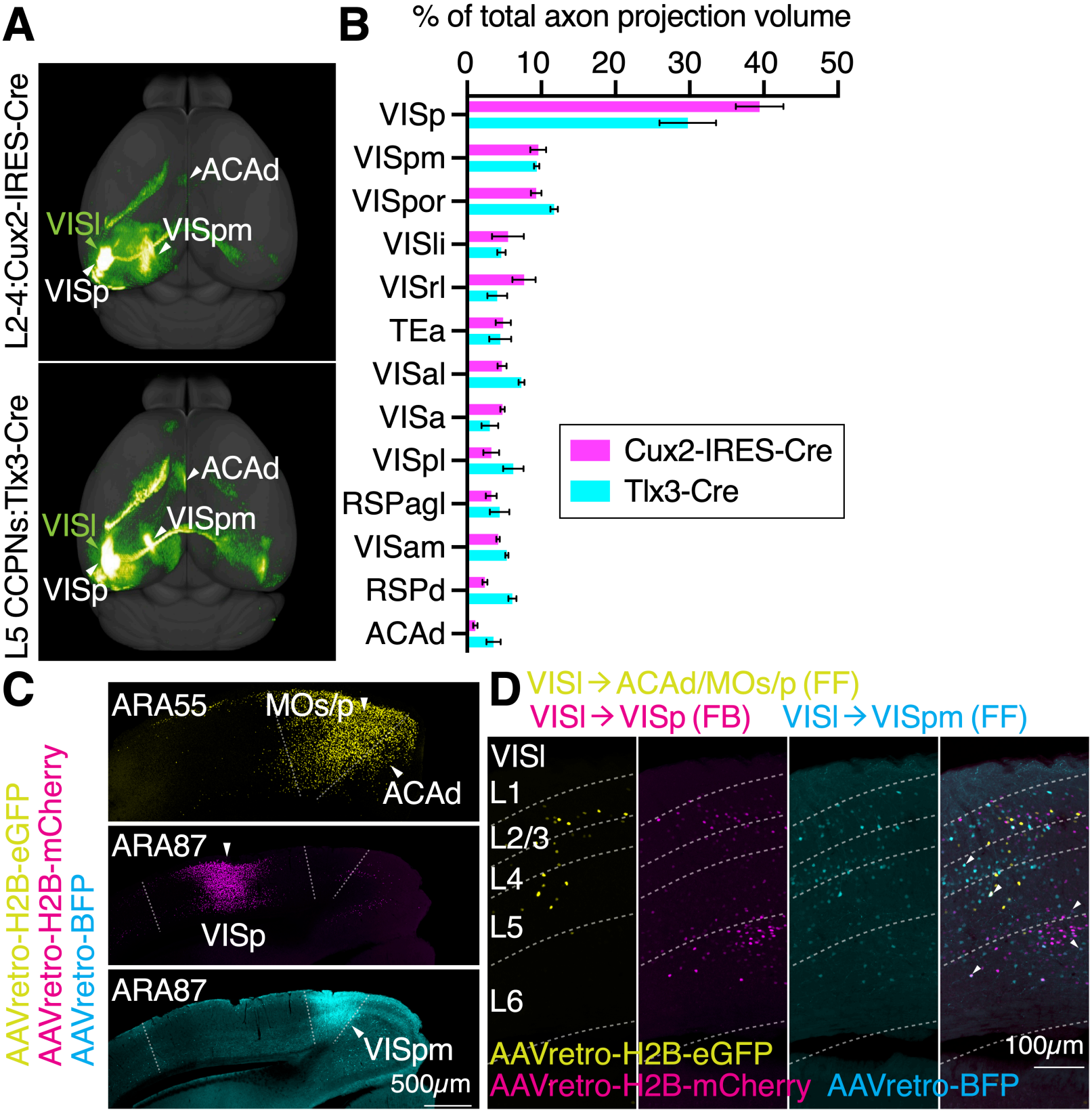
A
L2-4:Cux2-IRES-Cre
ACAd
VISl
VISpm
VISp
L5 CCPNs:Tlx3-Cre
ACAd
VISl
VISpm
VISp
B
% of total axon projection volume
0
10
20
30
40
50
VISp
VISpm
VISpor
VISli
VISrl
TEa
VISal
VISa
VISpl
RSPagl
VISam
RSPd
ACAd
Cux2-IRES-Cre
Tlx3-Cre
C
AAVretro-H2B-eGFP
AAVretro-H2B-mCherry
AAVretro-BFP
ARA55
MOs/p
ACAd
ARA87
VISp
ARA87
VISpm
500μm
D
VISl → ACAd/MOs/p (FF)
VISl → VISp (FB)
VISl → VISpm (FF)
VISl
L1
L2/3
L4
L5
L6
AAVretro-H2B-eGFP
AAVretro-H2B-mCherry
AAVretro-BFP
100μm

Figure 2

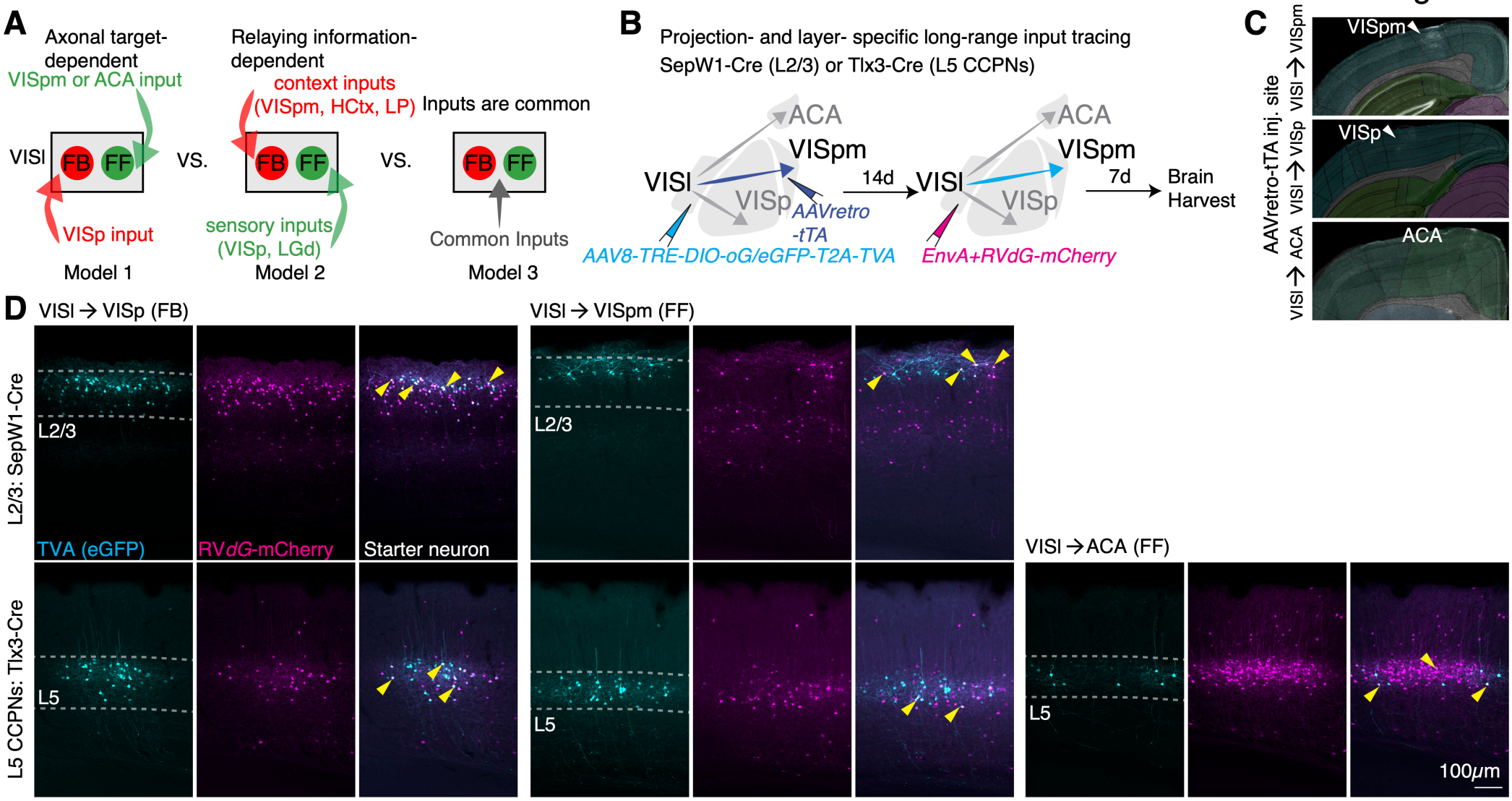
A
Axonal target-dependent
VISpm or ACA input
VISl
FB
FF
VISp input
Model 1
VS.
Relaying information-dependent
context inputs
(VISpm, HCtx, LP)
sensory inputs
(VISp, LGd)
Model 2
VS.
Inputs are common
Common Inputs
Model 3
B
Projection- and layer- specific long-range input tracing
SepW1-Cre (L2/3) or Tlx3-Cre (L5 CCPNs)
ACA
VISpm
VISl
VISp
AAVretro
-tTA
AAV8-TRE-DIO-oG/eGFP-T2A-TVA
14d
EnvA+RVdG-mCherry
7d
Brain
Harvest
C
AAVretro-tTA inj. site
VISl → VISpm
VISl → VISp
VISl → ACA
VISpm
VISp
ACA
D
VISl → VISp (FB)
VISl → VISpm (FF)
VISl → ACA (FF)
L2/3: SepW1-Cre
L5 CCPNs: Tlx3-Cre
L2/3
L5
TVA (eGFP)
RVdG-mCherry
Starter neuron
100μm

Figure 3

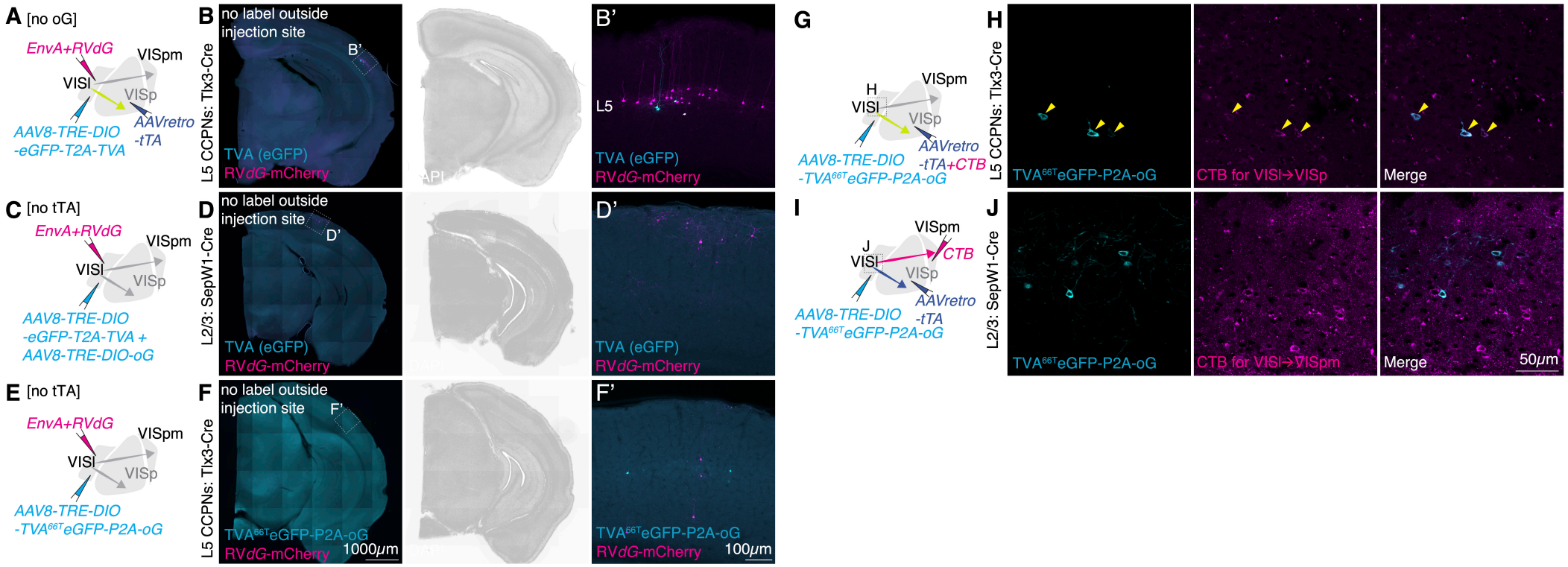
A [no oG]
EnvA+RVdG
VISpm
VISl
VISp
AAV8-TRE-DIO
-eGFP-T2A-TVA
AAVretro
-tTA
B
no label outside
injection site
B'
L5 CCPNs: Tlx3-Cre
TVA (eGFP)
RVdG-mCherry
L5
C [no tTA]
EnvA+RVdG
AAV8-TRE-DIO
-eGFP-T2A-TVA +
AAV8-TRE-DIO-oG
D
D'
L2/3: SepW1-Cre
E [no tTA]
AAV8-TRE-DIO
-TVA66TeGFP-P2A-oG
F
F'
TVA66TeGFP-P2A-oG
1000μm
100μm
G
H
AAVretro
-tTA+CTB
I
J
CTB
CTB for VISl→VISp
CTB for VISl→VISpm
Merge
50μm

Figure 4

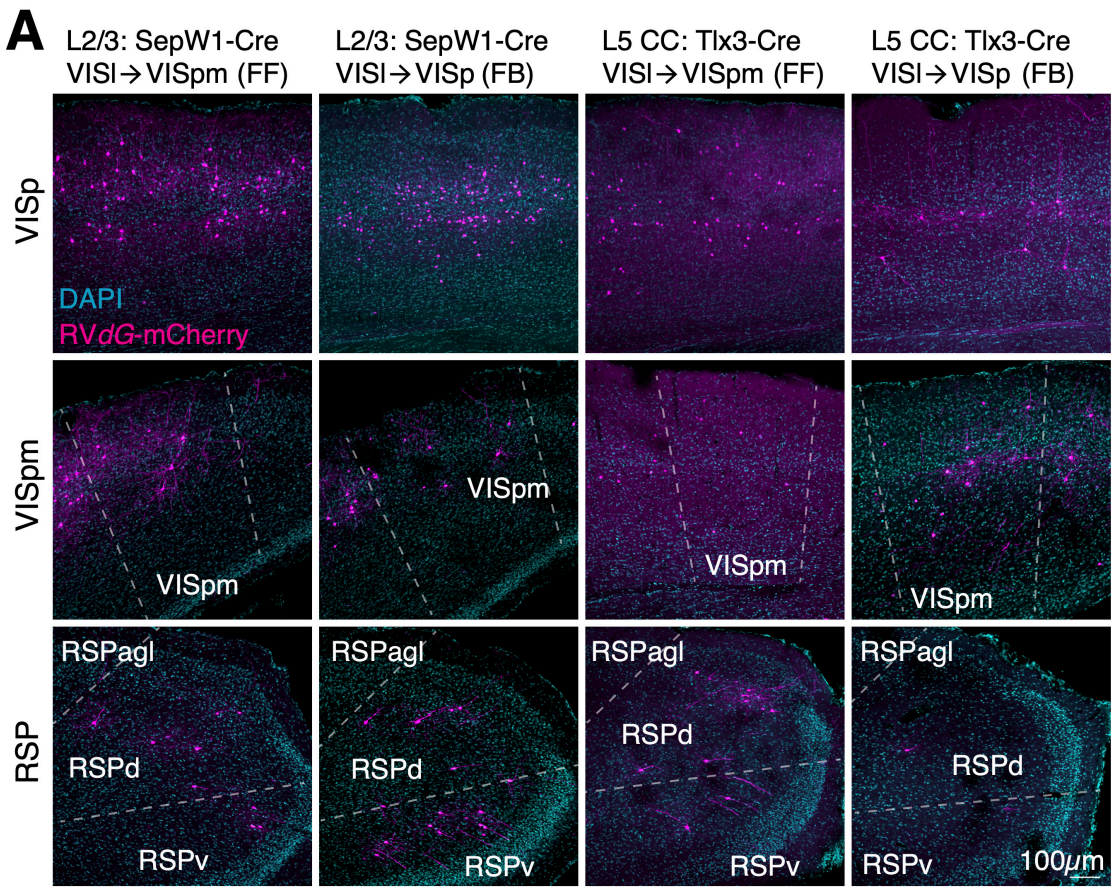
A
L2/3: SepW1-Cre
VISl→VISpm (FF)
L2/3: SepW1-Cre
VISl→VISp (FB)
L5 CC: Tlx3-Cre
VISl→VISpm (FF)
L5 CC: Tlx3-Cre
VISl→VISp (FB)
VISp
VISpm
RSP
DAPI
RVdG-mCherry
VISpm
RSPagl
RSPd
RSPv
100μm

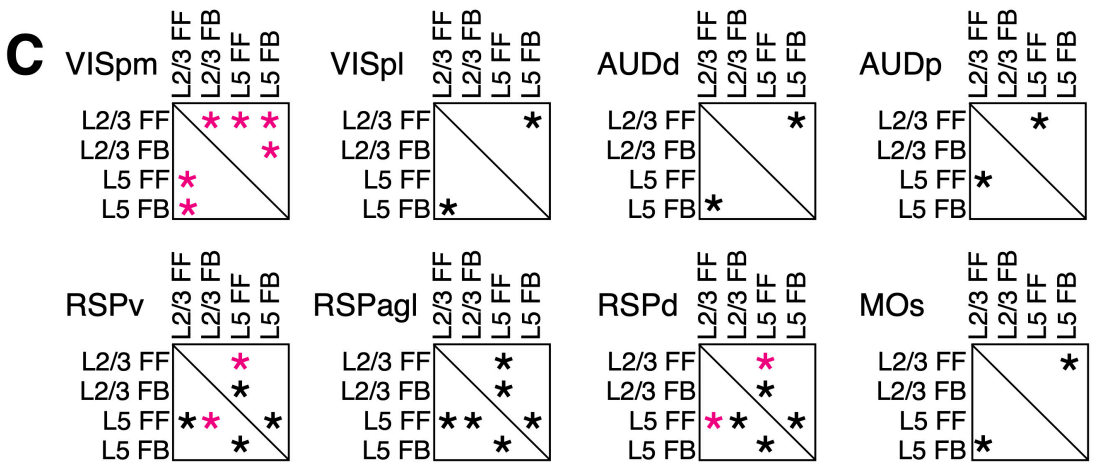
C
VISpm
VISpl
AUDd
AUDp
RSPv
RSPagl
RSPd
MOs
L2/3 FF
L2/3 FB
L5 FF
L5 FB

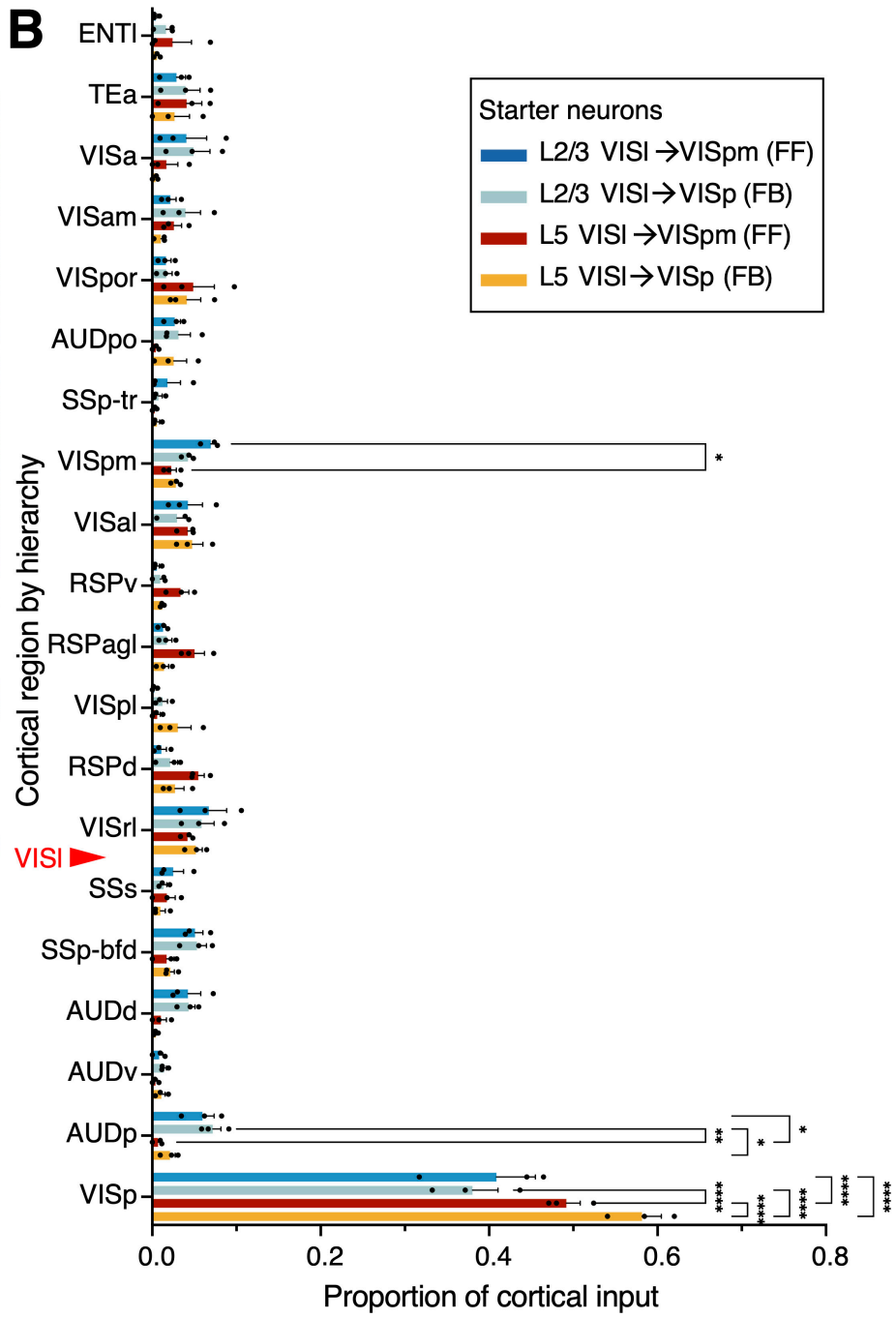
B
ENTl
TEa
VISa
VISam
VISpor
AUDpo
SSp-tr
VISpm
VISal
RSPv
RSPagl
VISpl
RSPd
VISrl
VISl
SSs
SSp-bfd
AUDd
AUDv
AUDp
VISp
Cortical region by hierarchy
Starter neurons
L2/3 VISl →VISpm (FF)
L2/3 VISl→VISp (FB)
L5 VISl →VISpm (FF)
L5 VISl→VISp (FB)
0.0
0.2
0.4
0.6
0.8
Proportion of cortical input

Figure 5

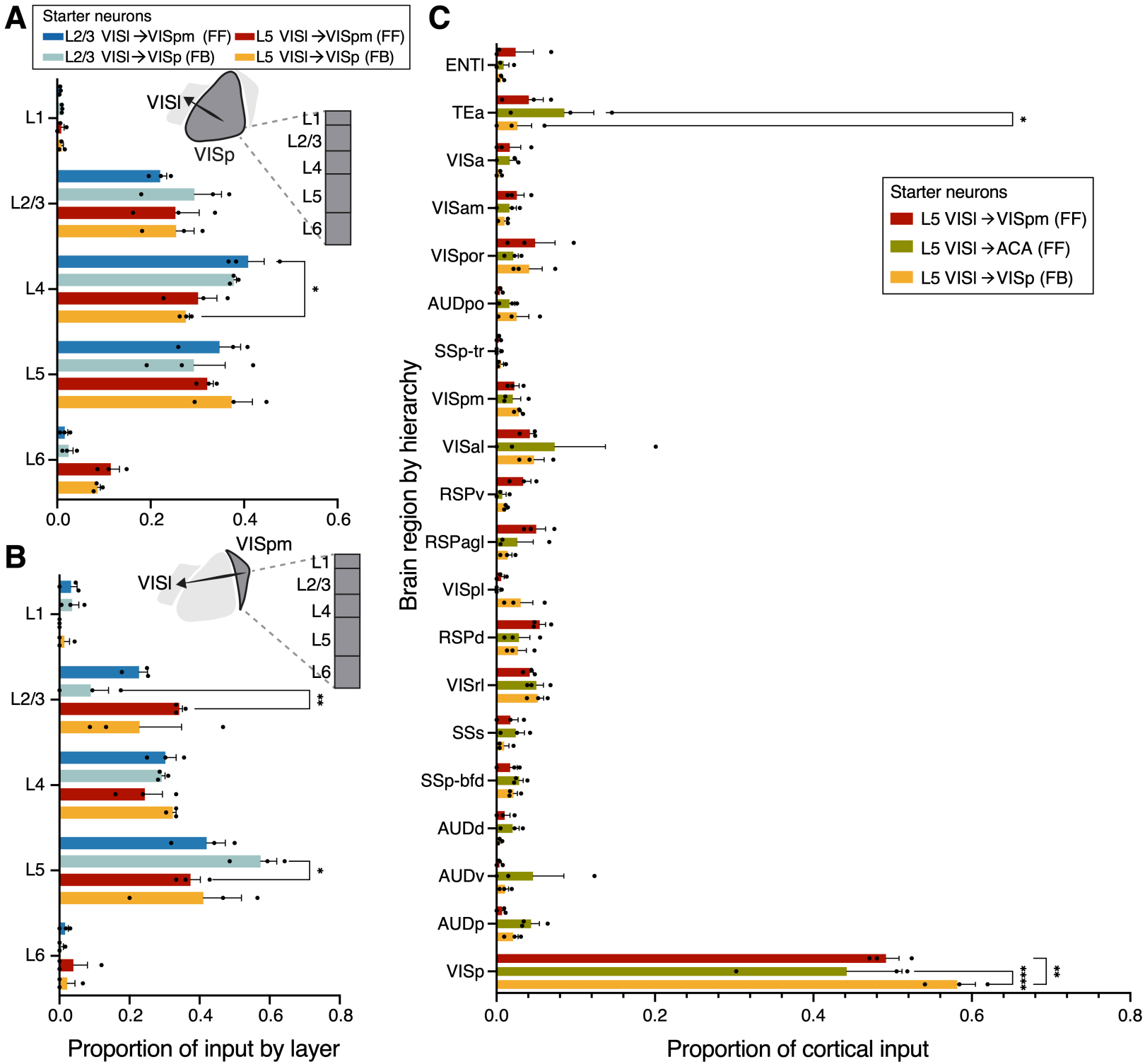
A
Starter neurons
L2/3 VISl →VISpm (FF)
L5 VISl →VISpm (FF)
L2/3 VISl→VISp (FB)
L5 VISl→VISp (FB)
VISl
VISp
L1
L2/3
L4
L5
L6
0.0
0.2
0.4
0.6
B
VISpm
VISl
0.8
Proportion of input by layer
C
ENTl
TEa
VISa
VISam
VISpor
AUDpo
SSp-tr
VISpm
VISal
RSPv
RSPagl
VISpl
RSPd
VISrl
SSs
SSp-bfd
AUDd
AUDv
AUDp
VISp
Brain region by hierarchy
Starter neurons
L5 VISl →VISpm (FF)
L5 VISl →ACA (FF)
L5 VISl →VISp (FB)
Proportion of cortical input

Figure 6

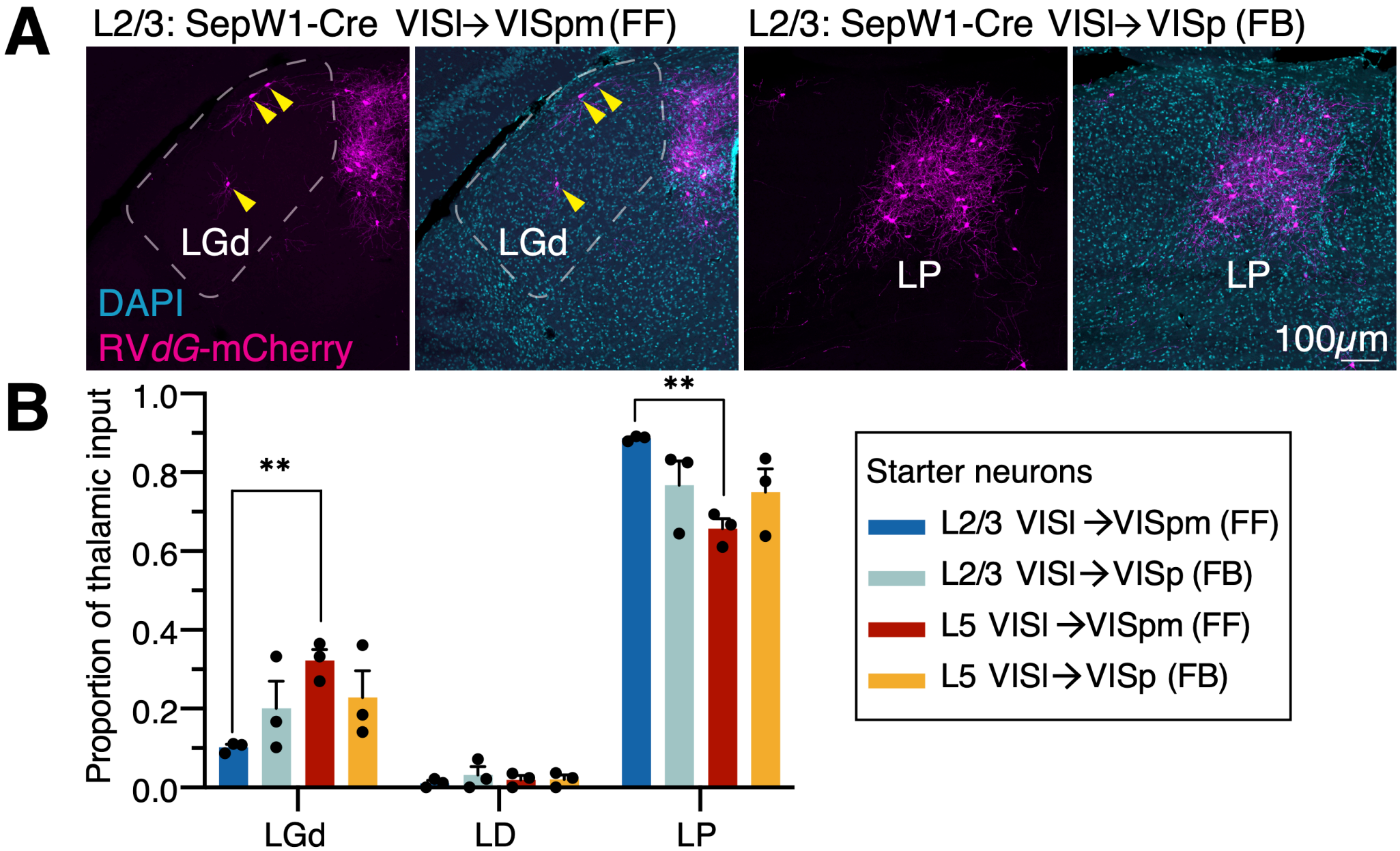
A
L2/3: SepW1-Cre VISl→VISpm (FF)
L2/3: SepW1-Cre VISl→VISp (FB)
LGd
LGd
LP
LP
DAPI
RVdG-mCherry
100μm
B
Proportion of thalamic input
1.0
0.8
0.6
0.4
0.2
0.0
**
**
LGd
LD
LP
Starter neurons
L2/3 VISl →VISpm (FF)
L2/3 VISl→VISp (FB)
L5 VISl →VISpm (FF)
L5 VISl→VISp (FB)

Raw counts in each brain area

Experiment	Mouse ID	VISp	AUDp	SSp-n	AUDv	SSp-ll	AUDd	SSp-un	SSp-ul	SSp-m	SSp-bfd	SSs	VISrl	RSPd	MOp	VISpl	RSPagl	RSPv	VISal	VISpm	SSp-tr	ORBl	AUDpo	VISpor	ACAv	VISam	VISa	ECT	MOs	PERI	TEa	Alp	GU	VISC	ACAd	ENTl	ENTm
L2/3 VISl-VISpm	326	660	129	1	32	12	151	16	13	0	144	103	69	16	11	3	14	5	40	161	102	3	78	31	2	23	183	2	17	0	18	0	2	4	15	18	3
L2/3 VISl-VISpm	327	1038	184	1	21	1	55	4	3	2	98	26	140	50	2	14	30	7	72	128	7	1	64	61	0	42	55	4	17	0	77	2	0	1	7	5	15
L2/3 VISl-VISpm	328	193	15	0	0	0	13	0	0	0	17	6	46	1	0	0	8	5	33	32	1	0	6	3	1	15	4	1	9	2	19	1	0	0	2	1	0
L2/3 VISl-VISp	60	94	23	0	3	0	14	0	0	0	14	2	14	1	0	1	2	0	11	11	1	0	15	4	0	8	12	1	0	0	10	0	0	0	1	6	5
L2/3 VISl-VISp	161	403	54	0	18	0	27	0	1	0	30	11	32	31	0	22	26	14	36	32	2	0	16	27	0	12	15	8	0	1	64	3	0	12	0	22	3
L2/3 VISl-VISp	329	1191	238	0	41	5	161	0	7	0	256	74	307	93	9	31	58	49	19	175	58	9	60	18	2	264	299	3	49	1	36	2	1	1	49	5	11
L5 VISl-VISpm	67	76	0	1	0	1	0	0	0	0	0	5	7	10	0	0	5	5	7	2	0	0	0	2	0	2	0	1	1	1	1	2	0	3	0	10	2
L5 VISl-VISpm	118	290	7	0	2	1	14	1	2	0	18	0	27	29	0	3	45	10	18	21	2	0	3	60	0	27	4	0	0	0	29	2	0	0	0	0	1
L5 VISl-VISpm	143	601	12	0	10	0	10	3	1	0	28	22	42	60	0	16	54	63	61	25	7	0	10	44	0	24	55	0	0	0	86	1	0	3	0	4	4
L5 VISl-VISp	63	226	4	7	8	4	3	0	0	0	13	9	22	20	0	4	10	6	30	14	5	0	1	9	2	6	2	0	0	0	0	2	0	1	2	4	0
L5 VISl-VISp	64	646	32	0	10	0	2	0	0	0	17	4	40	21	0	22	5	10	30	23	3	0	57	29	0	15	7	3	0	1	63	0	0	0	0	2	2
L5 VISl-VISp	122	308	12	1	2	3	2	0	0	0	9	2	34	7	0	32	7	6	22	15	1	0	10	39	0	1	0	0	0	0	10	0	0	1	0	3	0
L5 VISl-ACA	325	320	20	0	0	0	14	0	0	0	24	16	42	34	0	4	41	3	12	25	4	0	2	14	0	12	14	0	0	0	11	0	0	0	0	3	2
L5 VISl-ACA	356	103	7	0	3	0	1	1	0	0	5	1	9	2	0	0	1	0	41	2	0	0	4	2	0	0	0	0	1	0	19	0	0	1	0	0	1
L5 VISl-ACA	396	164	35	0	67	0	18	0	0	0	12	23	21	11	0	0	4	9	0	6	0	0	14	17	0	16	15	38	0	14	79	0	0	0	0	12	5

Proportion of ipsilateral cortical inputs

Experiment	Mouse ID	VISp	AUDp	SSp-n	AUDv	SSp-ll	AUDd	SSp-un	SSp-ul	SSp-m	SSp-bfd	SSs	VISrl	RSPd	MOp	VISpl	RSPagl	RSPv	VISal	VISpm	SSp-tr	ORBl	AUDpo	VISpor	ACAv	VISam	VISa	ECT	MOs	PERI	TEa	Alp	GU	VISC	ACAd	ENTl	ENTm
L2/3 VISl-VISpm	326	31.75%	6.20%	0.05%	1.54%	0.58%	7.26%	0.77%	0.63%	0.00%	6.93%	4.95%	3.32%	0.77%	0.53%	0.14%	0.67%	0.24%	1.92%	7.74%	4.91%	0.14%	3.75%	1.49%	0.10%	1.11%	8.80%	0.08%	0.82%	0.00%	0.87%	0.00%	0.10%	0.19%	0.72%	0.87%	0.14%
L2/3 VISl-VISpm	327	46.55%	8.25%	0.04%	0.94%	0.04%	2.47%	0.18%	0.13%	0.09%	4.39%	1.17%	6.28%	2.24%	0.09%	0.63%	1.35%	0.31%	3.23%	5.74%	0.31%	0.04%	2.87%	2.74%	0.00%	1.88%	2.47%	0.14%	0.76%	0.00%	3.45%	0.09%	0.00%	0.04%	0.31%	0.22%	0.67%
L2/3 VISl-VISpm	328	44.57%	3.46%	0.00%	0.00%	0.00%	3.00%	0.00%	0.00%	0.00%	3.93%	1.39%	10.62%	0.23%	0.00%	0.00%	1.85%	1.15%	7.62%	7.39%	0.23%	0.00%	1.39%	0.69%	0.23%	3.46%	0.92%	0.14%	2.08%	0.46%	4.39%	0.23%	0.00%	0.00%	0.46%	0.23%	0.00%
L2/3 VISl-VISp	60	37.30%	9.13%	0.00%	1.19%	0.00%	5.56%	0.00%	0.00%	0.00%	5.56%	0.79%	5.56%	0.40%	0.00%	0.40%	0.79%	0.00%	4.37%	4.37%	0.40%	0.00%	5.95%	1.59%	0.00%	3.17%	4.76%	0.19%	0.00%	0.00%	3.97%	0.00%	0.00%	0.00%	0.40%	2.38%	1.98%
L2/3 VISl-VISp	161	44.09%	5.91%	0.00%	1.97%	0.00%	2.95%	0.00%	0.11%	0.00%	3.28%	1.20%	3.50%	3.39%	0.00%	2.41%	2.84%	1.53%	3.94%	3.50%	0.22%	0.00%	1.75%	2.95%	0.00%	1.31%	1.64%	0.43%	0.00%	0.11%	7.00%	0.33%	0.00%	1.31%	0.00%	2.41%	0.33%
L2/3 VISl-VISp	329	33.28%	6.65%	0.00%	1.15%	0.14%	4.50%	0.00%	0.20%	0.00%	7.15%	2.07%	8.58%	2.60%	0.25%	0.87%	1.62%	1.37%	0.53%	4.89%	1.62%	0.25%	1.68%	0.50%	0.06%	7.38%	8.35%	0.07%	1.37%	0.03%	1.01%	0.06%	0.03%	0.03%	1.37%	0.14%	0.31%
L5 VISl-VISpm	67	53.52%	0.00%	0.70%	0.00%	0.70%	0.00%	0.00%	0.00%	0.00%	0.00%	3.52%	4.93%	7.04%	0.00%	0.00%	3.52%	3.52%	4.93%	1.41%	0.00%	0.00%	0.00%	1.41%	0.00%	1.41%	0.00%	0.36%	0.70%	0.00%	0.70%	1.41%	0.00%	2.11%	0.00%	7.04%	1.41%
L5 VISl-VISpm	118	47.08%	1.14%	0.00%	0.32%	0.16%	2.27%	0.16%	0.32%	0.00%	2.92%	0.00%	4.38%	4.71%	0.00%	0.49%	7.31%	1.62%	2.92%	3.41%	0.32%	0.00%	0.49%	9.74%	0.00%	4.38%	0.65%	0.00%	0.00%	0.00%	4.71%	0.32%	0.00%	0.00%	0.00%	0.00%	0.16%
L5 VISl-VISpm	143	48.23%	0.96%	0.00%	0.80%	0.00%	0.80%	0.24%	0.08%	0.00%	2.25%	1.77%	3.37%	4.82%	0.00%	1.28%	4.33%	5.06%	4.90%	2.01%	0.56%	0.00%	0.80%	3.53%	0.00%	1.93%	4.41%	0.00%	0.00%	0.00%	6.90%	0.08%	0.00%	0.24%	0.00%	0.32%	0.32%
L5 VISl-VISp	63	54.59%	0.97%	1.69%	1.93%	0.97%	0.72%	0.00%	0.00%	0.00%	3.14%	2.17%	5.31%	4.83%	0.00%	0.97%	2.42%	1.45%	7.25%	3.38%	1.21%	0.00%	0.24%	2.17%	0.48%	1.45%	0.48%	0.00%	0.00%	0.00%	0.00%	0.48%	0.00%	0.24%	0.48%	0.97%	0.00%
L5 VISl-VISp	64	62.06%	3.07%	0.00%	0.96%	0.00%	0.19%	0.00%	0.00%	0.00%	1.63%	0.38%	3.84%	2.02%	0.00%	2.11%	0.48%	0.96%	2.88%	2.21%	0.29%	0.00%	5.48%	2.79%	0.00%	1.44%	0.67%	0.13%	0.00%	0.10%	6.05%	0.00%	0.00%	0.00%	0.00%	0.19%	0.19%
L5 VISl-VISp	122	58.44%	2.28%	0.19%	0.38%	0.57%	0.38%	0.00%	0.00%	0.00%	1.71%	0.38%	6.45%	1.33%	0.00%	6.07%	1.33%	1.14%	4.17%	2.85%	0.19%	0.00%	1.90%	7.40%	0.00%	0.19%	0.00%	0.00%	0.00%	0.00%	1.90%	0.00%	0.00%	0.19%	0.00%	0.57%	0.00%
L5 VISl-ACA	325	51.86%	3.24%	0.00%	0.00%	0.00%	2.27%	0.00%	0.00%	0.00%	3.89%	2.59%	6.81%	5.51%	0.00%	0.65%	6.65%	0.49%	1.94%	4.05%	0.65%	0.00%	0.32%	2.27%	0.00%	1.94%	2.27%	0.00%	0.00%	0.00%	1.78%	0.00%	0.00%	0.00%	0.00%	0.49%	0.32%
L5 VISl-ACA	356	50.49%	3.43%	0.00%	1.47%	0.00%	0.49%	0.49%	0.00%	0.00%	2.45%	0.49%	4.41%	0.98%	0.00%	0.00%	0.49%	0.00%	20.10%	0.98%	0.00%	0.00%	1.96%	0.98%	0.00%	0.00%	0.00%	0.00%	0.49%	0.00%	9.31%	0.00%	0.00%	0.49%	0.00%	0.00%	0.49%
L5 VISl-ACA	396	30.26%	6.46%	0.00%	12.36%	0.00%	3.32%	0.00%	0.00%	0.00%	2.21%	4.24%	3.87%	2.03%	0.00%	0.00%	0.74%	1.66%	0.00%	1.11%	0.00%	0.00%	2.58%	3.14%	0.00%	2.95%	2.77%	7.01%	0.00%	2.58%	14.58%	0.00%	0.00%	0.00%	0.00%	2.21%	0.92%

nts in each thalaProportion of thalamic inputs

Experiment	Mouse ID	LGd	LD	LP	LGd	LD	LP
L2/3 VISl-VISpm	326	4	1	41	8.70%	2.17%	89.13%
L2/3 VISl-VISpm	327	9	1	73	10.84%	1.20%	87.95%
L2/3 VISl-VISpm	328	1	0	8	11.11%	0.00%	88.89%
L2/3 VISl-VISp	60	1	0	5	16.67%	0.00%	83.33%
L2/3 VISl-VISp	161	30	2	58	33.33%	2.22%	64.44%
L2/3 VISl-VISp	329	17	12	137	10.24%	7.23%	82.53%
L5 VISl-VISpm	67	3	0	6	33.33%	0.00%	66.67%
L5 VISl-VISpm	118	23	3	59	27.06%	3.53%	69.41%
L5 VISl-VISpm	143	46	3	77	36.51%	2.38%	61.11%
L5 VISl-VISp	63	5	1	21	18.52%	3.70%	77.78%
L5 VISl-VISp	64	17	3	101	14.05%	2.48%	83.47%
L5 VISl-VISp	122	13	0	23	36.11%	0.00%	63.89%
L5 VISl-ACA	325	NA	NA	NA	NA	NA	NA
L5 VISl-ACA	356	NA	NA	NA	NA	NA	NA
L5 VISl-ACA	396	NA	NA	NA	NA	NA	NA

Experiment	Mouse ID	Sex	Strain	From	Projection	Mouse age (P) at virus #1/#2 injection	Virus #1a (oG) and #1b (TVA)	Virus #1a (oG) titer	Virus #1b (TVA) titer	Virus #2 AAVretro	Virus #2 titer	Mouse age (P) at virus #3 injection	Virus #3 (rabies)	Virus #3 titer	Total virus/tracer incubation time (day)
FF/FB identity: Triple AAV	376	M	C57	VISI	ACA, VISp, VISpm	95	100 nl of scAAVretro-hSyn-H2B-eGFP into ACA, 100 nl of scAAVretro-hSyn-H2B-mCherry into VISp, 100 nl of AAVretro-BFP into VISpm	NA	NA	NA	NA	NA	NA	NA	18
FF/FB identity: Triple AAV	414	F	C57	VISI	ACA, VISp, VISpm	89	50 nl of scAAVretro-hSyn-H2B-eGFP into ACA, 50 nl of scAAVretro-hSyn-H2B-mCherry into VISp, 50 nl of AAVretro-BFP into VISpm	NA	NA	NA	NA	NA	NA	NA	21
FF/FB identity: Triple AAV	415	F	C57	VISI	ACA, VISp, VISpm	89	50 nl of scAAVretro-hSyn-H2B-eGFP into VISp, 50 nl of scAAVretro-hSyn-H2B-mCherry into VISpm, 50 nl of AAVretro-BFP into ACA	NA	NA	NA	NA	NA	NA	NA	21
FF/FB Identity: Double CTB	378	F	C57	VISI	VISpm, VISp	113	100 nl of CTB-647 in VISpm, 100 nl of CTB-555 in VISp	NA	NA	NA	NA	NA	NA	NA	4
FF/FB Identity: Double CTB	124	F	Tlx3-Cre	VISI	VISpm, VISp	104	50 nl of CTB-555 in VISpm, 50 nl of CTB-647 in VISp	NA	NA	NA	NA	NA	NA	NA	3
FF/FB Identity: Triple CTB	375	M	C57	VISI	ACA, VISp, VISpm	95	100 nl of CTB-647 in VISpm, 100 nl of CTB-555 in ACA, 100 nl of CTB-488 in VISp	NA	NA	NA	NA	NA	NA	NA	4
FF/FB Identity: Triple CTB	353	M	SepW1-Cre	VISI	ACA, VISp, VISpm	72	50 nl of CTB-647 in VISpm, 50 nl of CTB-555 in VISp, 50 nl of CTB-488 in ACA	NA	NA	NA	NA	NA	NA	NA	4
FF/FB Identity: Triple CTB	354	M	SepW1-Cre	VISI	ACA, VISp, VISpm	72	50 nl of CTB-555 in VISpm, 50 nl of CTB-488 in VISp, 50 nl of CTB-647 in ACA	NA	NA	NA	NA	NA	NA	NA	4
Control: No G-protein test	392	M	Tlx3-Cre	VISI	VISp	91	50 nl mixture of PBS and AAV8-TRE-DIO-eGFP-T2A-TVA into VISI	NA	7.00E+12	50 nl of AAVretro-nEF-lox66/71-tTA	4.86E+13	105	100 nl of EnvA+RVdG-mCherry into VISI	1.43E+10	21
Control: No G-protein test	406	M	Tlx3-Cre	VISI	VISp	139	50 nl mixture of PBS and AAV8-TRE-DIO-eGFP-T2A-TVA into VISI	NA	7.00E+12	50 nl of AAVretro-nEF-lox66/71-tTA	4.86E+13	153	100 nl of EnvA+RVdG-mCherry into VISI	1.43E+10	21
Control: No G-protein test	405	M	Tlx3-Cre	VISI	VISp	139	50 nl mixture of PBS and AAV8-TRE-DIO-eGFP-T2A-TVA into VISI	NA	7.00E+12	50 nl of AAVretro-nEF-lox66/71-tTA	4.86E+13	153	100 nl of EnvA+RVdG-mCherry into VISI	1.43E+10	21
Control: Colocalization AAV retro with CTB	386	F	Tlx3-Cre	VISI	VISp	126	50 nl of AAV8-TRE-DIO-TVA66TeGFP-P2A-oG into VISI. 50 nl of CTB-647 in VISpm, 50 nl of CTB-555 in VISp	7.44E+13	NA	50 nl of AAVretro-nEF-lox66/71-tTA	4.86E+13	126	NA	NA	14
Control: Colocalization AAV retro with CTB	403	F	SepW1-Cre	VISI	VISp	131	50 nl of AAV8-TRE-DIO-TVA66TeGFP-P2A-oG into VISI. 50 nl of CTB-647 in VISp, 50 nl of CTB-555 in VISpm	7.44E+13	NA	50 nl of AAVretro-nEF-lox66/71-tTA	4.86E+13	NA	NA	NA	14
Control: Colocalization AAV retro with CTB	343	F	Tlx3-Cre	VISI	VISpm	149	50 nl mixture of AAV8-TRE-DIO-oG and AAV8-TRE-DIO-GFP-T2A-TVA into VISI. 10 nl of CTB-647 into VISpm	2.36E+13	7.00E+12	50 nl of AAVretro-nEF-lox66/71-tTA	4.86E+13	163	100 nl of EnvA+RVdG-mCherry into VISI	7.71E+08	21
Control: Colocalization AAV retro with CTB	344	F	Tlx3-Cre	VISI	VISpm	140	50 nl mixture of AAV8-TRE-DIO-oG and AAV8-TRE-DIO-GFP-T2A-TVA into VISI. 10 nl of CTB-647 into VISpm	2.36E+13	7.00E+12	50 nl of AAVretro-nEF-lox66/71-tTA	4.86E+13	154	100 nl of EnvA+RVdG-mCherry into VISI	7.71E+08	21
Control: No TTA test	94	M	Tlx3-Cre	VISI	NA	337	50 nl of AAV8-TRE-DIO-TVA66TeGFP-P2A-oG into VISI	7.44E+13	NA	NA	NA	NA	NA	NA	21
Control: No TTA test	425	M	SepW1-Cre	VISI	NA	74	50 nl of AAV8-TRE-DIO-TVA66TeGFP-P2A-oG into VISI	7.44E+13	7.44E+13	NA	NA	84	100 nl of EnvA+RVdG-mCherry into VISI	7.11E+09	21
Control: No TTA test	427	F	SepW1-Cre	Vis	NA	63	50 nl mixture of AAV8-TRE-DIO-oG and AAV8-TRE-DIO-GFP-T2A-TVA	1.41E+14	7.00E+12	NA	NA	77	100 nl of EnvA+RVdG-mCherry into VISI	7.11E+09	21
Control: No TTA test	428	F	SepW1-Cre	Vis	NA	63	50 nl mixture of AAV8-TRE-DIO-oG and AAV8-TRE-DIO-GFP-T2A-TVA	1.41E+14	7.00E+12	NA	NA	77	100 nl of EnvA+RVdG-mCherry into VISI	7.11E+09	21
Control: No TTA test	429	F	Tlx3-Cre	VISI	NA	51	50 nl of AAV8-TRE-DIO-TVA66TeGFP-P2A-oG into VISI	7.44E+13	7.44E+13	NA	NA	65	100 nl of EnvA+RVdG-mCherry into VISI	7.11E+09	21
Control: No TTA test	432	F	Tlx3-Cre	VISI	NA	49	50 nl of AAV8-TRE-DIO-TVA66TeGFP-P2A-oG into VISI	7.44E+13	7.44E+13	NA	NA	63	100 nl of EnvA+RVdG-mCherry into VISI	7.11E+09	21
Rabies: L2/3 VISl-VISpm	326	M	SepW1-Cre	VISI	VISpm	73	50 nl mixture of AAV8-TRE-DIO-oG and AAV8-TRE-DIO-GFP-T2A-TVA into VISI	2.36E+13	7.00E+12	50 nl of AAVretro-nEF-lox66/71-tTA	4.86E+13	87	100 nl of EnvA+RVdG-mCherry into VISI	7.71E+08	21
Rabies: L2/3 VISl-VISpm	327	M	SepW1-Cre	VISI	VISpm	73	50 nl mixture of AAV8-TRE-DIO-oG and AAV8-TRE-DIO-GFP-T2A-TVA into VISI	2.36E+13	7.00E+12	50 nl of AAVretro-nEF-lox66/71-tTA	4.86E+13	87	100 nl of EnvA+RVdG-mCherry into VISI	7.71E+08	21
Rabies: L2/3 VISl-VISpm	328	M	SepW1-Cre	VISI	VISpm	73	50 nl mixture of AAV8-TRE-DIO-oG and AAV8-TRE-DIO-GFP-T2A-TVA into VISI	2.36E+13	7.00E+12	50 nl of AAVretro-nEF-lox66/71-tTA	4.86E+13	87	100 nl of EnvA+RVdG-mCherry into VISI	7.71E+08	21
Rabies: L2/3 VISl-VISp	329	M	SepW1-Cre	VISI	VISp	68	50 nl mixture of AAV8-TRE-DIO-oG and AAV8-TRE-DIO-GFP-T2A-TVA into VISI	2.36E+13	7.00E+12	50 nl of AAVretro-nEF-lox66/71-tTA	4.86E+13	82	100 nl of EnvA+RVdG-mCherry into VISI	7.71E+08	21
Rabies: L2/3 VISl-VISp	161	F	SepW1-Cre	VISI	VISp	67	50 nl mixture of AAV8-TRE-DIO-oG and AAV8-TRE-DIO-GFP-T2A-TVA	1.41E+14	7.00E+12	50 nl of AAVretro-nEF-lox66/71-tTA	4.86E+13	81	100 nl of EnvA+RVdG-mCherry into VISI	7.71E+08	21
Rabies: L2/3 VISl-VISp	60	F	SepW1-Cre	VISI	VISp	65	50 nl of AAV8-TRE-DIO-TVA66TeGFP-P2A-oG into VISI	7.44E+13	NA	100 nl of AAVretro-nEF-lox66/71-tTA	4.86E+13	79	100 nl of EnvA+RVdG-mCherry into VISI	1.78E+09	21
Rabies: L5 VISl-VISpm	67	F	Tlx3-Cre	VISI	VISpm	69	50 nl of AAV8-TRE-DIO-TVA66TeGFP-P2A-oG into VISI	7.44E+13	NA	50 nl of AAVretro-nEF-lox66/71-tTA	4.86E+13	83	100 nl of EnvA+RVdG-mCherry into VISI	1.07E+09	21
Rabies: L5 VISl-VISpm	143	M	Tlx3-Cre	VISI	VISpm	65	50 nl mixture of AAV8-TRE-DIO-oG and AAV8-TRE-DIO-GFP-T2A-TVA into VISI	1.41E+14	7.00E+12	50 nl of AAVretro-nEF-lox66/71-tTA	4.86E+13	79	100 nl of EnvA+RVdG-mCherry into VISI	7.71E+08	21
Rabies: L5 VISl-VISpm	118	F	Tlx3-Cre	VISI	VISpm	106	50 nl mixture of AAV8-TRE-DIO-oG and AAV8-TRE-DIO-GFP-T2A-TVA into VISI	1.41E+14	7.00E+12	50 nl of AAVretro-nEF-lox66/71-tTA	4.86E+13	120	100 nl of EnvA+RVdG-mCherry into VISI	1.07E+09	21
Rabies: L5 VISl-ACA	325	M	Tlx3-Cre	VISI	ACA	92	50 nl mixture of AAV8-TRE-DIO-oG and AAV8-TRE-DIO-GFP-T2A-TVA into VISI	2.36E+13	7.00E+12	50 nl of AAVretro-nEF-lox66/71-tTA	4.86E+13	106	100 nl of EnvA+RVdG-mCherry into VISI	7.71E+08	21
Rabies: L5 VISl-ACA	356	F	Tlx3-Cre	VISI	ACA	74	50 nl mixture of AAV8-TRE-DIO-oG and AAV8-TRE-DIO-GFP-T2A-TVA into VISI	2.36E+13	7.00E+12	50 nl of AAVretro-nEF-lox66/71-tTA	4.86E+13	89	100 nl of EnvA+RVdG-mCherry into VISI	7.71E+08	21
Rabies: L5 VISl-ACA	396	F	Tlx3-Cre	VISI	ACA	125	50 nl mixture of AAV8-TRE-DIO-oG and AAV8-TRE-DIO-GFP-T2A-TVA into VISI	1.41E+14	7.00E+12	50 nl of AAVretro-nEF-lox66/71-tTA	4.86E+13	139	100 nl of EnvA+RVdG-mCherry into VISI	1.43E+10	21
Rabies: L5 VISl-VISp	122	F	Tlx3-Cre	VISI	VISp	97	50 nl mixture of AAV8-TRE-DIO-oG and AAV8-TRE-DIO-GFP-T2A-TVA into VISI	1.41E+14	7.00E+12	50 nl of AAVretro-nEF-lox66/71-tTA	4.86E+13	111	100 nl of EnvA+RVdG-mCherry into VISI	1.07E+09	21
Rabies: L5 VISl-VISp	63	M	Tlx3-Cre	VISI	VISp	70	50 nl of AAV8-TRE-DIO-TVA66TeGFP-P2A-oG into VISI	7.44E+13	NA	200 nl of AAVretro-nEF-lox66/71-tTA	4.86E+13	84	100 nl of EnvA+RVdG-mCherry into VISI	1.78E+09	21
Rabies: L5 VISl-VISp	64	F	Tlx3-Cre	VISI	VISp	71	50 nl of AAV8-TRE-DIO-TVA66TeGFP-P2A-oG into VISI	7.44E+13	NA	100 nl of AAVretro-nEF-lox66/71-tTA	4.86E+13	85	100 nl of EnvA+RVdG-mCherry into VISI	1.07E+09	21